

Analysis and Detection of RIS-based Spoofing in Integrated Sensing and Communication (ISAC)

Tingyu Shui, *Graduate Student Member, IEEE*, Po-Heng Chou, *Member, IEEE*, Walid Saad, *Fellow, IEEE*, and Mingzhe Chen, *Senior Member, IEEE*

Abstract—Integrated sensing and communication (ISAC) is a key feature of next-generation 6G wireless systems, allowing them to achieve high data rates and sensing accuracy. While prior research has primarily focused on addressing communication safety in ISAC systems, the equally critical issue of sensing safety remains largely under-explored. In this paper, the possibility of spoofing the sensing function of ISAC in vehicle networks is examined, whereby a malicious reconfigurable intelligent surface (RIS) is deployed to compromise the sensing functionality of a roadside unit (RSU). For this scenario, the requirements on the malicious RIS' phase shifts design and number of reflecting elements are analyzed. Under such spoofing, the practical estimation bias of the vehicular user (VU)'s Doppler shift and angle-of-departure (AoD) for an arbitrary time slot is analytically derived. Moreover, from the attacker's view, a Markov decision process (MDP) is formulated to optimize the RIS's phase shifts design. The goal of this MDP is to generate complete and plausible fake trajectories by incorporating the concept of spatial-temporal consistency. To defend against this sensing spoofing attack, a signal temporal logic (STL)-based neuro-symbolic attack detection framework is proposed and shown to learn interoperable formulas for identifying spoofed trajectories. Simulation results show that, with a beam misalignment of only 3.1° , a spoofed velocity can be estimated with a significant deviation from -9.9 m/s to 50 m/s, when the ground truth is 10 m/s. Moreover, an AoD estimation bias of up to 11° can be induced by the attacker. Such spoofed sensing outcomes cause a 28% reduction in the achievable rate of the VU in the beam tracking application. Finally, the proposed attack detection framework achieves an accuracy of 74.17% in identifying the RIS attack, which is 53.34% higher than that of a deep clustering-based benchmark.

Index Terms—ISAC, Sensing safety, Vehicular network, RIS.

I. INTRODUCTION

To realize future intelligent transportation systems (ITS), communications between transportation agents (vehicle and/or infrastructure) are fundamental for safety-critical applications such as cooperative perception and autonomous driving. Particularly, a vehicular network will need both sensing and communication services of high reliability and quality. One promising approach is integrated sensing and communication (ISAC) [1], which equips vehicle and infrastructure with simultaneous communication and sensing capability.

ISAC enables the integration of communication and sensing functions in ITS through the co-design of the hardware architecture, transmitted waveforms, and signal processing algorithms on connected autonomous vehicle (CAV) and roadside unit (RSU) [2]. Such joint design benefits the vehicular network via two distinct aspects: communication aided sensing

(CAS) and sensing aided communication (SAC) [3]. First, for CAS, the sensing accuracy and coverage can be enhanced by leveraging inter-agent transmission of environment perception information. One example is cooperative perception in which vehicles can extend their perception coverage by sharing the local sensing outcomes via wireless communication [4]. Correspondingly, SAC aims to exploit the sensing outcome to improve communication performance. Particularly, the sensing outcome pertaining to communication users, e.g., high-mobility vehicular users (VUs), can assist the transceiver to achieve accurate beam alignment and meet desired communication quality-of-service (QoS) at high-frequency bands [5]. However, such highly coupled design can be vulnerable to malicious attacks due to the broadcast nature of wireless transmission [6]. Given the dire consequences of faulty sensing information in both CAS and SAC applications, it is essential to design ISAC systems that can still operate effectively under adversarial conditions.

Aligned with the dual ISAC functionalities, the security concerns in an ISAC system should also be addressed from two distinct perspectives: *communication safety* and *sensing safety*. Generally, works on *communication safety* [7]–[9] reconsider the basic attacks in wireless communication, e.g., eavesdropping and jamming, in the context of ISAC. Therein, the goal is to ensure confidential transmission while considering the tight coupling of sensing and communication functionalities. However, the *sensing safety* issue in ISAC systems remains largely under-explored. Some preliminary works are presented in [10]–[13], in which the objective is, from a defender's perspective, to prevent attackers from accessing the sensing information of authorized targets. Specifically, inspired by electronic countermeasure (ECM) techniques, these works [10]–[13] leverage a reconfigurable intelligent surface (RIS) to enhance the sensing echoes received at the authorized ISAC station while suppressing those received at the unauthorized ISAC station. Although the exploitation of RIS improves the *sensing safety* of ISAC systems, this strategy also raises critical questions: *Can an RIS be adversarially deployed by an attacker to compromise the sensing safety of ISAC systems instead? If so, how would this malicious RIS be designed, and what impact would it have on the sensing outcomes? Can we design ISAC systems resilient to such an attack on sensing functionality?*

A. Prior Works

The issue of sensing safety has recently attracted interest in a number of prior works [10]–[18]. Specifically, in [10]–[12] the authors used an RIS, as a legitimate component, to enhance the sensing safety of ISAC systems by providing confidential sensing service. The phase shifts and amplitudes of the RIS, mounted on the target, are deliberately designed for directional

T. Shui and W. Saad are with Bradley Department of Electrical and Computer Engineering, Virginia Tech, Alexandria, VA, 22305, USA, Emails: tygrady@vt.edu, walids@vt.edu.

Po-Heng Chou is with the Research Center for Information Technology Innovation, Academia Sinica, Taipei, 11529, Taiwan, Email: d00942015@ntu.edu.tw.

M. Chen is with the Department of Electrical and Computer Engineering and Frost Institute for Data Science and Computing, University of Miami, Coral Gables, FL, 33146, USA, Email: mingzhe.chen@miami.edu.

radar stealth. As a result, the targets can only be detected by the authorized ISAC station, while remaining invisible to unauthorized ISAC station. In [13], the RIS was further exploited to simultaneously conceal the target and even spoof the unauthorized ISAC station by redirecting the detection signal to clutter. As a result, a deceptive angle-of-arrival (AoA) sensing outcome is generated at the unauthorized ISAC station.

Meanwhile, the authors in [14]–[18] examined the potential of sensing attacks, which aim to generate faulty sensing outcomes at the authorized ISAC station by manipulating the sensing echoes. In [14], a sensing-resistant jammer was designed to disrupt the legitimate transmission while concealing itself from being detected. A novel metric named angular-domain peak-to-average ratio (ADPAR) is proposed to quantify the detectability of the jammer. Then, the achievable rate of legitimate transmission is minimized under ADPAR constraints. However, compared with active jamming, passive attacks pose greater challenges. In [15], the authors examined the impact of “DISCO” RIS, i.e., a malicious RIS with random and time-varying reflection properties, on the ISAC system. Moreover, the work in [15] provided a theoretical analysis on the lower bound of the signal-to-interference-plus-noise ratio (SINR) received by the communication users under the considered attack. In addition, the works in [16] and [17] further experimentally implemented backscatters tags for sensing attacks. In [18], the authors extended the scenario to multiple jamming attackers and further proposed an attack detection method. In particular, in [18], a two-stage transmission protocol is designed, where beam scanning is used for attack detection in the first stage and a robust jamming beamforming is designed in the second stage to mitigate the impact of sensing attack.

While some prior works [10]–[18] have examined the sensing safety issue in ISAC systems, a number of challenges remain unaddressed and require further investigation. Firstly, the prior art generally quantifies the impact of sensing attack by lower-bound metrics such as the Cramér-Rao bound (CRB), which reflect the theoretical limit of sensing accuracy. However, this overlooks the practical estimation bias introduced by spoofing attacks, which is critical for downstream tasks like beam tracking and trajectory planning. Secondly, none of the existing studies has examined spoofed sensing outcomes from a trajectory-level perspective. In particular, the existing literature only focuses on the impact of sensing spoof within a single time slot. Thus, when a full trajectory composed of multiple time slots is given, such a temporally isolated anomaly can be easily detected due to its inconsistency with adjacent time slots. In contrast, if a spoofing attack is capable of generating a complete plausible trajectory, it can greatly increase the severity of its impact and make detection significantly more challenging. Thirdly, the prior art, such as in [10]–[18], does not develop efficient detection mechanisms for sensing attacks on ISAC systems. In our preliminary work [19], we studied the feasibility of the RIS sensing attack for a vehicular network in which the goal of the RIS is to manipulate the sensing echo received by the RSU. The practical estimation bias of the VU’s Doppler shift and angle-of-departure (AoD) are analytically derived. However, our work in [19] only

focuses on the spoofed sensing outcomes within a single time slot and does not examine the possibility of the malicious RIS to generate plausible trajectories. Furthermore, the framework in [19] does not provide any solution for attack detection in such spoofing use cases.

B. Contributions

The main contribution of this paper is, thus, the analysis of the impact of malicious RIS on the sensing safety of ISAC systems and the development of a corresponding attack detection framework. We particularly investigate the feasibility of RIS spoofing on the RSU’s estimation of a VU’s Doppler shift and AoD. The necessary conditions for the RIS to conduct the spoofing are derived and the practical estimation bias of the sensing outcomes are analyzed, from both slot-level and trajectory-level perspectives. Finally, a signal temporal logic (STL)-based neuro-symbolic attack detection framework is proposed to identify spoofed trajectories. To our best knowledge, *this is the first work that studies the feasibility of sensing attacks launched by malicious RIS, analyzes its impact on sensing outcomes, and proposes a corresponding attack detection approach.* Hence, our key contributions include:

- We consider a novel RIS-aided spoofing scenario in which the sensing safety of an ISAC vehicular network is compromised. We derive the necessary conditions on the RIS, i.e. time-varying phase shifts and number of reflecting elements, of such a spoofing attack. We derive its impact on the RSU’s estimation bias of the VU’s Doppler shift and AoD. Specifically, the feasible spoofing frequencies set with respect to the VU’s Doppler shift for each single sensing slot is derived. Moreover, we analytically show that, the maximum likelihood estimator (MLE) of the AoD will also be jeopardized under the proposed RIS spoofing.
- From the attacker’s perspective, we formulate a Markov decision process (MDP) optimization problem that allows the attacker to design the RIS’ phase shifts in a way to generate complete and plausible fake trajectories that are difficult to distinguish from regular, real-world ones. Particularly, we define and incorporate the concept of spatial-temporal consistency into the MDP, serving as a regularization term to ensure that the spoofed trajectory adheres to real-world physical constraints across consecutive time slots. This makes it challenging for the RSU to identify the spoofed trajectories and detect the existence of a malicious RIS. Due to the state-dependent action space of the proposed MDP, an action-masking enhanced proximal policy optimization (PPO) framework is deployed on the attacker.
- From a defender’s view, we propose an STL-based neuro-symbolic learning framework that detects potential sensing attacks by investigating the sensed VU’s trajectory. In particular, STL is a formal language used to specify the temporal properties of time signal sequence. By leveraging the TLINet approach of [20], we explicitly learn the formulas that a real-world trajectory should satisfy, which is then used to identify abnormal spoofed trajectory. Finally, an interpretable sensing attack detection mechanism can be realized according to the learned formulas.

- Simulation results demonstrate that the RIS spoofing attack significantly compromises the sensing accuracy and the communication performance of the VU. Specifically, with a beam misalignment of only 3.1° , the estimation error of the VU's velocity can range from -9.9 m/s to 50 m/s, when the ground truth is 10 m/s, and, an AoD estimation bias of up to 11° can be induced. Due to the spoofed sensing outcomes, the achievable rate of the VU will be decreased by 28% in the beam tracking application. Moreover, compared to the deep clustering-based detection benchmark, our proposed framework improves the detection accuracy by 53.34% , achieving a final accuracy of 74.17% in identifying the RIS attack.

The rest of the paper is organized as follows. The system model is presented in Section II. The impact of the RIS spoofing on the sensing outcome in a single time slot is analyzed in Section III. Section IV extends the analysis to trajectory level. Section V introduces the STL-based neuro-symbolic attack detection framework. Section VI presents the simulation results and Section VII concludes the paper.

II. SYSTEM MODEL

Consider an ISAC system supported by a full-duplex millimeter wave (mmWave) RSU [5]. The RSU is equipped with a uniform linear array (ULA) of N_t transmit antennas and N_r receive antennas to provide sensing and downlink communications to a single-antenna VU. By estimating the VU's kinetic states from echo signals, the RSU can support critical applications such as beam tracking and safety alert. Following the standard convention in [5], we consider a scenario in which the VU moves along a multi-lane straight road parallel to the RSU's ULA.¹ A two-dimensional Cartesian coordinate system is used with the RSU located at its origin, as shown in Fig. 1. We focus on a time period discretized into K short time slots, i.e., sensing time slots, and assume that each time slot corresponds to a short interval T . During time slot k , the goal of the RSU is to estimate the VU's coordinates (x_k, y_k) and velocity v_k ,² which are assumed to be constant in a given time slot [22]. Thus, the RSU can obtain the VU's trajectory $\mathcal{S} = [s_1, \dots, s_K]$ with $s_k = [x_k, y_k, v_k]^T$. In this considered system, a malicious RIS is deployed to compromise the RSU's sensing functionality by manipulating the echo signals. Without loss of generality, we next introduce the system model with respect to time slot k .

A. Signal Model

Let $q_k(t) \in \mathbb{C}$ be the RSU's transmitted ISAC symbol at time t during slot k with unit power, i.e., $q_k(t)q_k^*(t) = 1$. Given the precoding vector $\mathbf{w}_k \in \mathbb{C}^{N_t \times 1}$ at the RSU, the echo signal reflected by the VU will be given by:

$$\mathbf{y}_{V,k}(t) = \sqrt{P}\gamma_B\beta_{V,k}e^{j2\pi\mu_k t}\mathbf{b}_B(\theta_k)\mathbf{a}_B^H(\theta_k)\mathbf{w}_kq_k(t - \tau_k), \quad (1)$$

where P is the transmit power of the RSU, $\gamma_B = \sqrt{N_t N_r}$ is the array gain factor, and $\beta_{V,k} = \sqrt{\frac{\lambda^2 \kappa_V}{64\pi^3 d_k^4}} e^{\frac{j4\pi d_k}{\lambda}}$ combines

¹The extension to non-parallel cases is straightforward and can be done by rotating the coordinate system.

²The velocity v_k captures only the x-directional component. The y-axis component can be either estimated by deploying another ULA aligned with the y-axis or inferred from the uplink information transmitted by the VU [21].

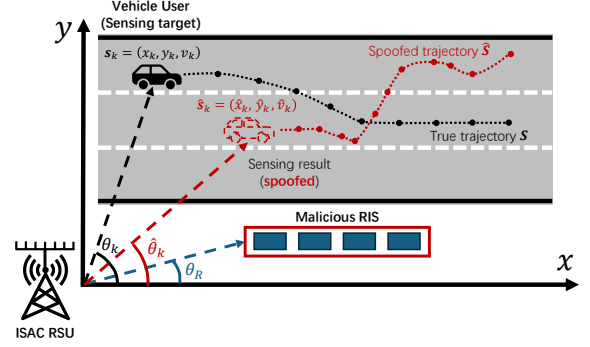


Fig. 1. Illustration of the considered ISAC system model under the spoofing of a malicious RIS.

the complex path gain of the RSU-VU-RSU link and the radar cross section (RCS) κ_V of the VU [23]. The distance between the RSU and the VU is d_k and the carrier wavelength is λ . Meanwhile, the Doppler shift μ_k , AoD θ_k , and double-path echo delay τ_k of the VU are included in (1), where $\mathbf{a}_B(\theta)$ and $\mathbf{b}_B(\theta)$ are the steering vectors of the transmitting and receiving antennas, respectively, at the RSU. By assuming a half-wavelength antenna space, $\mathbf{a}_B(\theta)$ and $\mathbf{b}_B(\theta)$ will be given by [5]:

$$\mathbf{a}_B(\theta) = \frac{1}{\sqrt{N_t}} [1, e^{-j\pi \cos \theta}, \dots, e^{-j\pi(N_t-1) \cos \theta}]^T, \quad (2)$$

$$\mathbf{b}_B(\theta) = \frac{1}{\sqrt{N_r}} [1, e^{-j\pi \cos \theta}, \dots, e^{-j\pi(N_r-1) \cos \theta}]^T. \quad (3)$$

In presence of the malicious RIS, the echo received by the RSU is a composition of the legitimate echo reflected by the VU and the spoofing echo adversarially reflected by the RIS. We assume that the RIS is equipped with a ULA of M elements. Thus, the spoofing echo from the RIS will be:

$$\mathbf{y}_{R,k}(t) = \sqrt{P}\gamma_B\beta_R\mathbf{b}_R(\theta_R)\mathbf{a}_R^H(\theta_B)\text{diag}[\phi_k(t)] \times \mathbf{b}_R(\theta_B)\mathbf{a}_R^H(\theta_R)\mathbf{w}_kq_k(t - \tau_R), \quad (4)$$

where $\beta_R = \sqrt{\frac{\lambda^2 \kappa_R}{64\pi^3 d_R^4}} e^{\frac{j4\pi d_R}{\lambda}}$ combines the complex path gain of the RSU-RIS-RSU link and the RCS κ_R of the RIS. According to [11], we have $\kappa_R = \frac{4\pi\eta S^2}{\lambda^2}$ with the RIS's reflection efficiency η , area S , and operating wavelength λ . Similarly, $\mathbf{b}_R(\cdot)$ and $\mathbf{a}_R(\cdot)$, θ_B , and τ_R are the steering vectors, AoA (and also AoD), and echo delay of the RIS. The phase shifts at the RIS are given by $\phi_k(t) = [e^{j\phi_{k,1}(t)}, \dots, e^{j\phi_{k,M}(t)}]$ and unit reflection amplitudes are assumed for simplicity. Note that $\phi_k(t)$ must be time-varying to spoof the sensing process, as we will explain in Section III-A. Thus, the composite echo received by the RSU will be given by:

$$\mathbf{y}_k(t) = \mathbf{y}_{R,k}(t) + \mathbf{y}_{V,k}(t) + \mathbf{z}_E(t), \quad (5)$$

where $\mathbf{z}_E(t) \sim \mathcal{CN}(0, \sigma^2 \mathbf{I}_M)$ is the additive white Gaussian noise (AWGN) at the RSU's receiving antennas.

B. Sensing Model

The goal of the sensing process on the RSU during time slot k is to estimate $[\tau_k, \mu_k, \theta_k]$ for deriving s_k . Particularly, the RSU can determine μ_k and θ_k through a standard matched-filtering technique [5], after which the received signal in (5) is compensated in both time and frequency domain for further

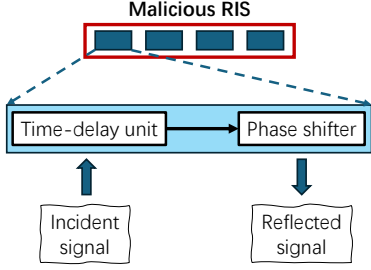


Fig. 2. The architecture of the adjustable-delay RIS.

estimating θ_k . In particular, the matched-filtering output of $\mathbf{y}_k(t)$ is defined as follows:

$$C_k(\tau, \mu) \triangleq \left| \int_0^T \mathbf{y}_k(t) q^*(t - \tau) e^{-j2\pi\mu t} dt \right|^2. \quad (6)$$

Thus, the estimated echo delay and Doppler shift can be given by $(\hat{\tau}_k, \hat{\mu}_k) = \arg \max_{\tau, \mu} C_k(\tau, \mu)$. Moreover, we consider the MLE of θ_k , defined as:

$$\hat{\theta}_k = \arg \max_{\theta_k} p(\hat{\mathbf{y}}_k | \theta_k). \quad (7)$$

In (7), $p(\hat{\mathbf{y}}_k | \theta_k)$ represents the likelihood function and $\hat{\mathbf{y}}_k = \int_0^T \mathbf{y}_k(t) q^*(t - \hat{\tau}_k) e^{-j2\pi\hat{\mu}_k t} dt$ is the echo compensated by $\hat{\tau}_k$ and $\hat{\mu}_k$. Given $[\hat{\tau}_k, \hat{\mu}_k, \hat{\theta}_k]$, we can estimate \mathbf{s}_k :

$$\hat{\mathbf{s}}_k = \left[c\hat{\tau}_k \cos \hat{\theta}_k, c\hat{\tau}_k \sin \hat{\theta}_k, \frac{\hat{\mu}_k c}{f_c \cos \hat{\theta}_k} \right]. \quad (8)$$

The goal of the malicious RIS is to hinder the RSU from obtaining accurate $[\hat{\tau}_k, \hat{\mu}_k, \hat{\theta}_k]$, thereby degrading the accuracy of $\hat{\mathbf{s}}_k$. In other words, the spoofing echo $\mathbf{y}_{R,k}(t)$ given in (4) is expected to cause a deviation in the peak position of $C_k(\tau, \mu)$ and further distort the accuracy of the MLE $\hat{\theta}_k$. In a typical ISAC system with large bandwidth, the delay resolution of $C_k(\tau, \mu)$ is sufficiently high to resolve the two echoes given in (1) and (4). Thus, the spoofed echo can be mitigated if the echo delay difference satisfies $|\tau_k - \tau_R| \geq \tau_0$, where τ_0 is the effective main-lobe width of $C_k(\tau, \mu)$ in the time domain. To successfully conduct the echo spoofing, an adjustable-delay RIS [24] is assumed in our system, as shown in Fig. 2. Specifically, a time-delay unit is cascaded before the RIS's phase shifter such that it is able to store and retrieve the impinging signals with a designed delay Δt_R . As a result, the echo delay in (4) will be: $\tau_R = \Delta t_R + 2\frac{d_R}{c}$.

Remark 1. The reason for incorporating the adjustable-delay RIS is to ensure that $|\tau_k - \tau_R| < \tau_0$. In other words, $\hat{\tau}_k$ is not spoofed. Hereinafter, we consider $|\tau_k - \tau_R| \approx 0$ since τ_0 , inversely proportional to the bandwidth [25], is typically small in ISAC systems (e.g., 2 ns with bandwidth of 500 MHz [22]). Thus, a necessary condition for the RIS echo spoofing is $d_R \leq d_k \leq d_R + \frac{\Delta_{\max} c}{2}$ with Δ_{\max} being the maximum adjustable-delay. For instance, given a typical value $\Delta_{\max} = 0.32$ us [24], the spoofing range becomes $d_R \leq d_k \leq d_R + 48$ m.

Equipped with the time-delay unit, the malicious RIS can manipulate the sensing echo received at the RSU. Next, we derive the key conditions on the RIS, i.e., its phase shifts design, for conducting the considered spoofing attack. Moreover, the spoofing attack's impact on the VU's sensing outcomes within time slot k is analyzed.

III. SLOT-LEVEL IMPACT OF SENSING SPOOFING

In this section, we examine the conditions on the malicious RIS's phase shift design for a successful spoofing attack. From the slot-level perspective, we derive the feasible spoofing frequency set on the VU's Doppler shift estimation. Moreover, we further analyze the practical AoD estimation bias.

A. Conditions on RIS's Phase shifts

First, we can rewrite the matched-filtering output in (6) as:

$$C_k(\tau, \mu) = \left| \sqrt{P} \gamma_B \beta_{V,k} \mathbf{b}_B(\theta_k) \mathbf{a}_B^H(\theta_k) \mathbf{w}_k c_{V,k}(\tau, \mu) + \sqrt{P} \gamma_B \beta_R \mathbf{b}_B(\theta_R) \mathbf{a}_B^H(\theta_R) \mathbf{w}_k c_{R,k}(\tau, \mu) + \tilde{\mathbf{z}}_E(\tau, \mu) \right|^2, \quad (9)$$

where $c_{V,k}(\tau, \mu) \triangleq \int_0^T q(t - \tau_k) q^*(t - \tau) e^{-j2\pi(\mu - \mu_k)t} dt$, $c_{R,k}(\tau, \mu) \triangleq \int_0^T q(t - \tau_k) q^*(t - \tau) \left[\sum_{m=1}^M e^{-j(2\pi\mu t - \phi_{k,m}(t))} \right] dt$, and $\tilde{\mathbf{z}}_E(\tau, \mu) \triangleq \int_0^T \mathbf{z}_E(t) q^*(t - \tau) e^{-j2\pi\mu t} dt$. To spoof the sensing outcome, we assume that the RIS can derive $\Delta t_R = \tau_R - 2\frac{d_R}{c}$ by eavesdropping on the uplink communication of the VU, which is a reasonable assumption [23]. Thus, $C_k(\tau, \mu)$ will only exhibit one peak around τ_k in the time domain. Moreover, we assume a perfect echo delay estimation $\hat{\tau}_k = \tau_k$ due to the high delay resolution in large bandwidth mmWave ISAC systems. In other words, we only focus on the spoofed estimation of μ_k and θ_k .

Given (9), we can observe that the impact of RIS spoofing stems from the term $\sqrt{P} \gamma_B \beta_R \mathbf{b}_B(\theta_R) \mathbf{a}_B^H(\theta_R) \mathbf{w}_k c_{R,k}(\tau, \mu)$. Assuming $\hat{\tau}_k = \tau_k$, we have $c_{V,k}(\hat{\tau}_k, \mu) = \int_0^T e^{-j2\pi(\mu - \mu_k)t} dt$ and $c_{R,k}(\hat{\tau}_k, \mu) = \sum_{m=1}^M \int_0^T e^{-j(2\pi\mu t - \phi_{k,m}(t))} dt$. We can find that the peak position of $c_{V,k}(\hat{\tau}_k, \mu)$ in the frequency domain occurs at $\mu = \mu_k$. Thus, it is natural to set $\phi_{k,m}(t) = 2\pi\tilde{\mu}_{k,m}t$ for artificially creating M peak positions at frequencies $\tilde{\mu}_{k,1}, \dots, \tilde{\mu}_{k,M}$. In practice, due to the hardware constraints of the RIS, the phase shift $\phi_{k,m}(t)$ on the m -th element can be only given in a discrete form as:

$$\phi_{k,m}(t) = (2\pi\tilde{\mu}_{k,m} \lceil \frac{t}{\Delta T} \rceil \Delta T) \bmod 2\pi, \quad (10)$$

where ΔT represents the shortest time interval over which $\phi_{k,m}(t)$ can vary. Meanwhile, the modulo operation is applied because the phase shifts of the RIS are typically confined to the range 0 to 2π . Given the design in (10), we focus on one fundamental spoofing case in which the M spoofing frequencies are set equal, i.e., $\tilde{\mu}_{k,1} = \dots = \tilde{\mu}_{k,M} = \tilde{\mu}_k$ such that $\tilde{\mu}_k \triangleq \arg \max_{\mu} C_k(\hat{\tau}_k, \mu)$ is spoofed as $\tilde{\mu}_k$. Note that, by setting all M spoofing frequencies equal, the RIS coordinates all its elements coherently to construct a peak of maximum magnitude at $C_k(\hat{\tau}_k, \tilde{\mu}_k)$, which constitutes a simple yet effective strategy to spoof the Doppler shift estimation. To this end, the RIS should select $\tilde{\mu}_k$ such that the peak of $C_k(\hat{\tau}_k, \mu)$ occurs at $\tilde{\mu}_k$ rather than μ_k , i.e., $C_k(\hat{\tau}_k, \tilde{\mu}_k) \geq C_k(\hat{\tau}_k, \mu_k)$.

B. Impact on Sensing Outcomes

1) *Doppler Shift Estimation:* We begin by deriving the feasible spoofing frequency set $\mathcal{A}_k \triangleq \{\tilde{\mu}_k | C_k(\hat{\tau}_k, \tilde{\mu}_k) \geq C_k(\hat{\tau}_k, \mu_k)\}$. Since the matched-filtering output of noise is

negligible compared to the spoofing echo, we can ignore $\tilde{z}_E(\hat{\tau}_k, \mu)$ and rewrite $C_k(\hat{\tau}_k, \mu)$ as:

$$C_k(\hat{\tau}_k, \mu) = \frac{PT^2\gamma_B^2}{N_r} \sum_{n_r=1}^{N_r} \left| \beta_{V,k} g_{n_r}(\theta_{0,k}, \theta_k) e^{-j\pi(\mu-\mu_k)T} \times \right. \\ \left. \text{sinc}(T(\mu-\mu_k)) + \beta_R g_{n_r}(\theta_{0,k}, \theta_R) M e^{j\pi\tilde{\mu}_k\Delta T} \times \right. \\ \left. e^{-j\pi(\mu-\tilde{\mu}_k)T} \text{sinc}(\mu\Delta T) f(K, \pi\Delta T(\mu-\tilde{\mu}_k)) \right|^2, \quad (11)$$

where we adopt a precoding vector $\mathbf{w}_k = \mathbf{a}_B(\theta_{0,k})$ steered towards $\theta_{0,k}$, which may be selected from a predefined codebook [26]. Moreover, in (11), we define $f(K, x) = \frac{\sin(Kx)}{K \sin x}$, $\text{sinc}(x) = \frac{\sin(\pi x)}{\pi x}$, and $g_{n_r}(\theta_1, \theta_2) = e^{-\frac{j\pi}{2}[\cos\theta_1(N_t-1) - \cos\theta_2(N_t+1-2n_r)]} f(N_t, \frac{\pi}{2}(\cos\theta_1 - \cos\theta_2))$. To derive the expression of \mathcal{A}_k , we first present the following lemma pertaining to a set of infeasible spoofing frequencies.

Lemma 1. *If the number of RIS reflecting elements satisfies $M \gg \sqrt{\frac{\kappa_V \lambda}{4\pi\eta S}} \left| \frac{f(N_t, \frac{\pi}{2}(\cos\theta_{0,k} - \cos\theta_k))}{f(N_t, \frac{\pi}{2}(\cos\theta_{0,k} - \cos\theta_R))} \right|$, an infeasible spoofing frequency set based on (11) can be given by $\mathcal{A}_{k,\emptyset} = \{\mu \mid \mu = \mu_k + \frac{n}{\Delta T}, n \in \mathbb{Z}\}$, i.e., $\mathcal{A}_{k,\emptyset} \cap \mathcal{A}_k = \emptyset$.*

Proof. See the proof in the conference version [19]. \square

Given Lemma 1, if we only consider $\tilde{\mu}_k \in \mathcal{A}_k$, i.e., $\tilde{\mu}_k \notin \mathcal{A}_{k,\emptyset}$, $C_k(\hat{\tau}_k, \mu)$ in (11) can be approximated by:

$$C_k(\hat{\tau}_k, \mu) \approx PT^2\gamma_B^2 \left[C_{V,k} \text{sinc}^2(T(\mu-\mu_k)) + M^2 C_R \times \right. \\ \left. \text{sinc}^2(\mu\Delta T) f^2(K, \pi\Delta T(\mu-\tilde{\mu}_k)) \right], \quad (12)$$

where the cross-product terms in the quadratic expansion are ignored since $f(K, \pi\Delta T(\mu-\tilde{\mu}_k)) \text{sinc}(T(\mu-\mu_k)) \approx 0$, $\forall \mu$ when $\tilde{\mu}_k \notin \mathcal{A}_{k,\emptyset}$. In (12), we further define $C_{V,k} \triangleq \beta_{V,k}^2 f^2(N_t, \frac{\pi}{2}(\cos\theta_{0,k} - \cos\theta_k))$ and $C_R \triangleq \beta_R^2 f^2(N_t, \frac{\pi}{2}(\cos\theta_{0,k} - \cos\theta_R))$. Another observation in (12) is that the impact of the spoofing frequency $\tilde{\mu}_k$ is periodic, as shown in the periodic spoofing term $M^2 C_R \text{sinc}^2(\mu\Delta T) f^2(K, \pi\Delta T(\mu-\tilde{\mu}_k))$. Specifically, the spoofing frequency $\tilde{\mu}_k$ will lead to multiple peaks at $\mu = \tilde{\mu}_k + \frac{n}{\Delta T}, n \in \mathbb{Z}$. Therefore, in order to derive \mathcal{A}_k , we only consider the highest peak defined in Lemma 2.

Lemma 2. *If the condition on M in Lemma 1 is satisfied, the highest peak of the spoofing term in (12) will be given by $\Delta\tilde{\mu}_k \triangleq \tilde{\mu}_k \bmod \frac{1}{\Delta T}$.*

Proof. See the proof in the conference version [19]. \square

Given the result in Lemma 2, the possible spoofing frequency is restricted to the range $(0, \frac{1}{\Delta T}]$. In other words, an RIS capable of changing its phase shift more frequently, i.e., operating with a smaller ΔT , will have a broader range of spoofing frequencies $\Delta\tilde{\mu}$. Moreover, the feasible spoofing frequency set should be redefined as $\mathcal{A}_k \triangleq \{\Delta\tilde{\mu}_k \mid C_k(\hat{\tau}_k, \Delta\tilde{\mu}_k) \geq C_k(\hat{\tau}_k, \mu_k)\}$, which is derived next.

Theorem 1. *Under the condition on M in Lemma 1, the feasible spoofing frequency set \mathcal{A}_k is given in (13).*

Proof. See the proof in the conference version [19]. \square

Theorem 1 shows that, if the RIS selects a spoofing frequency $\Delta\tilde{\mu}_k \in \mathcal{A}_k$, the estimated Doppler shift will be spoofed as $\hat{\mu}_k = \Delta\tilde{\mu}_k$. According to the derived result in (13), the range of feasible spoofing frequencies expands as more reflecting elements are deployed at the RIS. In addition, the beam orientation $\theta_{0,k}$ also influences the set \mathcal{A}_k . Generally, when $\theta_{0,k}$ is closer to the VU's AoD θ_k , the spoofing set \mathcal{A}_k becomes narrower, whereas a beam direction closer to the RIS's AoD θ_R leads to a wider set. This phenomenon poses a critical challenge when ISAC is leveraged for beam tracking. For instance, when a VU moves through the coverage of the RSU, there inevitably exists moments when the beam is steered closer to the RIS. At such instances, the RIS can select a spoofing frequency $\Delta\tilde{\mu}_k$ that results significant beam misalignment in the subsequent tracking step. More critically, this misalignment may accumulate over time, leading the RSU to lose track of the VU eventually and thereby jeopardizing the ISAC sensing process.

2) *Impact on AoD MLE:* Given the estimated $\hat{\tau}_k$ and $\hat{\mu}_k$, the RSU will continue to estimate θ_k . First, the compensated and normalized echo is given by:

$$\hat{\mathbf{y}}_k \triangleq \frac{1}{\sqrt{P}\gamma_B} \int_0^T \mathbf{y}_k(t) q^*(t - \hat{\tau}_k) e^{-j2\pi\Delta\tilde{\mu}_k t} dt. \quad (14)$$

We next define a perfect MLE $\tilde{\theta}_k$ obtained without spoofing and examine the deviation between the spoofed MLE $\hat{\theta}_k$ and $\tilde{\theta}_k$. First, we rewrite (14) as:

$$\hat{\mathbf{y}}_k = T\beta_{V,k} \mathbf{b}_B(\theta_k) h(\theta_k, \theta_{0,k}) e^{-j\pi(\Delta\tilde{\mu}_k - \mu_k)T} \times \\ \text{sinc}(T(\Delta\tilde{\mu}_k - \mu_k)) + MT\beta_R \mathbf{b}_B(\theta_R) \times \\ h(\theta_R, \theta_{0,k}) e^{j\pi\Delta\tilde{\mu}_k\Delta T} \text{sinc}(\Delta\tilde{\mu}_k\Delta T) + \hat{\mathbf{z}}_E, \quad (15)$$

where $\hat{\mathbf{z}}_E = \frac{\tilde{\mathbf{z}}_E(\hat{\tau}, \Delta\tilde{\mu}_k)}{\sqrt{P}\gamma_B} \sim \mathcal{CN}(\mathbf{0}_{N_r}, \frac{\sigma^2 T}{P\gamma_B^2} \mathbf{I}_{N_r})$ and $h(\theta_1, \theta_2) = e^{-\frac{j\pi(N_t-1)}{2}[\cos\theta_1 - \cos\theta_2]} f(N_t, \frac{\pi}{2}(\cos\theta_1 - \cos\theta_2))$. Similar to (7), we define the perfect MLE as follows:

$$\tilde{\theta}_k = \arg \max_{\theta_k} p(\tilde{\mathbf{y}}_k \mid \theta_k), \quad (16)$$

where $\tilde{\mathbf{y}}_k = T\beta_{V,k} \mathbf{b}_B(\theta_k) h(\theta_k, \theta_{0,k}) + \hat{\mathbf{z}}_E$. Here, $\tilde{\mathbf{y}}_k$ represents the normalized received signal compensated by perfect estimation $\hat{\tau}_k = \tau_k$ and $\hat{\mu}_k = \mu_k$, without the RIS spoof. Thus, $\tilde{\theta}_k$ in (16) is the best MLE on θ_k we can obtain.

Next, we derive the deviation between the perfect MLE $\tilde{\theta}_k$ and the spoofed MLE $\hat{\theta}_k$ in the following theorem.

Theorem 2. *Assume the perfect delay estimation $\hat{\tau}_k = \tau_k$ and spoofed Doppler shift estimation $\hat{\mu}_k = \Delta\tilde{\mu}$ are obtained under RIS spoofing. The spoofed MLE $\hat{\theta}_k$ can be given by:*

$$\hat{\theta}_k = \arg \min_{\theta_k} \left[\|\tilde{\mathbf{y}}_k - T\beta_{V,k} \mathbf{b}_B(\theta_k) h(\theta_k, \theta_{0,k})\|^2 + \right. \\ \left. 2T\beta_{V,k} \sum_{n=1}^{N_r} \Re\{\Delta y_{k,n} g_n^*(\theta_k, \theta_{0,k})\} \right], \quad (17)$$

where $\Delta \mathbf{y}_k \triangleq \tilde{\mathbf{y}}_k - \tilde{\mathbf{y}}_k = [\Delta y_{k,1}, \dots, \Delta y_{k,N_r}]^T$. Moreover, the perfect MLE $\tilde{\theta}_k$ defined in (16) can be similarly given by:

$$\tilde{\theta}_k = \arg \min_{\theta_k} \|\tilde{\mathbf{y}}_k - T\beta_{V,k} \mathbf{b}_B(\theta_k) h(\theta_k, \theta_{0,k})\|^2. \quad (18)$$

$$\mathcal{A}_k = \{\Delta\tilde{\mu}_k \mid M^2 C_R [\text{sinc}^2(\Delta\tilde{\mu}_k \Delta T) - \text{sinc}^2(\mu_k \Delta T) f^2(K, \pi \Delta T (\mu_k - \Delta\tilde{\mu}_k))] - C_{V,k} [1 - \text{sinc}^2(T(\mu_k - \Delta\tilde{\mu}_k))] \geq 0\}. \quad (13)$$

Proof. See the proof in the conference version [19]. \square

From Theorem 2, we can observe that the spoofed MLE deviates from the perfect MLE because of the term $2T\beta_{V,k} \sum_{n=1}^{N_r} \Re\{\Delta y_{k,n} g_n^*(\theta_k, \theta_{0,k})\}$, which is introduced by the malicious RIS. Although it is challenging to derive a closed-form expression for $|\hat{\theta}_k - \tilde{\theta}_k|$, we can still find that a spoofed MLE $\hat{\theta}_k \neq \tilde{\theta}_k$ will be obtained if the location of the minimum of $\|\hat{\mathbf{y}} - T\beta_{V,k} \mathbf{b}_B(\theta_k) h(\theta_k, \theta_{0,k})\|^2$ is altered due to the addition of the term $2T\beta_{V,k} \sum_{n=1}^{N_r} \Re\{\Delta y_{k,n} g_n^*(\theta_k, \theta_{0,k})\}$. To further illustrate the impact of RIS spoofing on the AoD estimation, we derive $\Delta \mathbf{y}_k$ as follows:

$$\begin{aligned} \Delta \mathbf{y}_k &= T\beta_{V,k} \mathbf{b}_B(\theta_k) h(\theta_k, \theta_{0,k}) \times \\ &\quad \left[e^{-j\pi(\Delta\tilde{\mu}_k - \mu_k)T} \text{sinc}(T(\Delta\tilde{\mu}_k - \mu_k)) - 1 \right] \\ &\quad + MT\beta_R \mathbf{b}_B(\theta_R) h(\theta_R, \theta_{0,k}) e^{j\pi\Delta\tilde{\mu}_k \Delta T} \text{sinc}(\Delta\tilde{\mu}_k \Delta T). \end{aligned} \quad (19)$$

From (19), we can observe that the RIS's impact on the AoD estimation stems from the second term. Particularly, given the same spoofing frequency $\Delta\tilde{\mu}$, an RIS with a larger number of reflecting elements M , higher path gain β_R , and an AoD θ_R closer to the RSU's beam direction $\theta_{0,k}$ tends to induce more significant AoD estimation bias.

Theorems 1 and 2 explicitly demonstrate estimation bias of $\hat{\theta}_k$ and $\hat{\mu}_k$ for an arbitrary time slot k . However, when a full trajectory composed of multiple time slots is considered, a single spoofed sensing outcome can be easily detected due to its inconsistency with adjacent time slots. Therefore, from the attacker's view, we next examine the feasibility of such RIS spoofing from a trajectory-level perspective, with the goal of generating complete and plausible fake trajectories.

IV. TRAJECTORY-LEVEL IMPACT OF SENSING SPOOFING

In this section, we further investigate the phase shift design of the RIS for spoofing a complete trajectory at the RSU. Specifically, from the attacker's perspective, the objective is to generate a plausible trajectory that satisfies real-world spatial-temporal consistency, thereby increasing the difficulty of attack detection. To this end, we formulate an MDP for optimizing the spoofing frequency sequence on the RIS, and solve it using a PPO framework enhanced with action mask.

A. Problem Formulation

The aim of the malicious RIS is to select the spoofing frequency to induce spoofed trajectory $\hat{\mathbf{S}} = [\hat{s}_1, \dots, \hat{s}_K]$ at the RSU, with $\hat{s}_k = [\hat{x}_k, \hat{y}_k, \hat{v}_k]$. In practice, the regular trajectory of a VU should follow certain spatial and temporal consistency. Thus, to generate plausible sensing outcomes that cannot be easily identified, the spoofing frequency sequence $\Delta\tilde{\mu} = [\Delta\tilde{\mu}_1, \dots, \Delta\tilde{\mu}_K]$ should be designed carefully.

We begin by defining the spatial and temporal consistency of a trajectory. Formally, a trajectory $\mathbf{S} = [s_1, \dots, s_K]$ with $s_k \in \mathbb{R}^m$ follows spatial and temporal consistency when a vector-valued constraint $c(s_k, s_{k+1}) : \mathbb{R}^m \times \mathbb{R}^m \rightarrow \mathbb{R}^n$ satisfies $c(s_k, s_{k+1}) \succeq \mathbf{0}$ for all $k \in \{1, \dots, K-1\}$. Here, the expression of constraint $c(\cdot, \cdot)$ and dimension n are both related to the physical law that a real-world trajectory should

follow. For instance, a VU is subject to physical constraints on acceleration. Thus, the constraint $c(s_k, s_{k+1}) \succeq \mathbf{0}$ may encode condition $v_{k+1} - v_k \leq a_{\max} T$, where a_{\max} is the maximum acceleration. To formulate a comprehensive $c(s_k, s_{k+1})$ is challenging since the physical constraints in real world can be complicated. For tractability, we consider a simplified but practical consistency:

$$c(s_k, s_{k+1}) = \begin{bmatrix} a_{\max} T - (v_{k+1} - v_k) \\ (v_{k+1} - v_k) - a_{\min} T \\ \delta_x - \|x_{k+1} - x_k - v_k T\| \\ \delta_y - \|y_{k+1} - y_k\| \end{bmatrix}, \quad (20)$$

where a_{\min} is the minimum acceleration (maximum deceleration), δ_x is the estimation error margin along x-axis, and δ_y is the estimation error margin along y-axis. The first two terms in (20) capture the change in the VU's velocity between adjacent steps, while the last two terms represent the change in the VU's location. Thus, we can formulate the spoofing frequency design as a feasibility problem given by:

$$\text{find } \Delta\tilde{\mu} \in \mathbb{R}^T \quad (21a)$$

$$\text{s.t. } \Delta\tilde{\mu}_k \in \mathcal{A}_k, \forall k = 1, \dots, K, \quad (21b)$$

$$c(\hat{s}_k, \hat{s}_{k+1}) \succeq \mathbf{0}, \forall k = 0, \dots, K-1, \quad (21c)$$

where (21b) indicates that the spoofing frequency at each time slot should be selected from the corresponding feasible spoofing frequency set and (21c) ensures that the spatial temporal consistency is satisfied for the whole trajectory. Moreover, we assume an accurate initial sensing, i.e., $\hat{s}_0 = s_0$.

B. MDP with State-dependent Action Mask

The feasibility problem (21) can be interpreted as a sequential decision-making process. Specifically, the RIS needs to determine its spoofing frequency $\Delta\tilde{\mu}_k$ at time slot k to generate spoofed sensing outcome \hat{s}_k . Moreover, the consistency constraint given in (21c) should be satisfied to ensure a plausible trajectory at the RSU. Note that the RIS only needs to know the true state s_k of the VU to perform such spoofing (as detailed later in this section), and this state can be easily obtained through the uplink transmission of the VU [23]. To solve (21), we next map it into an MDP and propose a reinforcement learning (RL)-based approach.

First, we establish the first-order Markov property of the sequential decision-making process by defining its action $\Delta\tilde{\mu}$ and state $\xi_k = [\hat{s}_{k-1}, s_k]$, where \hat{s}_{k-1} is the spoofed sensing outcome at time slot $k-1$ and s_k is the true state of VU at time slot k . Our goal is to show that the future state ξ_{k+1} depends only on the current state ξ_k and action $\Delta\tilde{\mu}_k$, and is conditionally independent of past states and actions. Recall that the spoofed sensing outcome under $\Delta\tilde{\mu}_k \in \mathcal{A}_k$ in (8) is given as $\hat{s}_k = \left[c\tau_k \cos \hat{\theta}_k, c\tau_k \sin \hat{\theta}_k, \frac{\Delta\tilde{\mu}_k c}{f_c \cos \hat{\theta}_k} \right]$, where $\hat{\theta}_k$ is determined by the sensing outcome \hat{s}_{k-1} , the true state s_k of VU, and the beam direction $\theta_{0,k}$ according to Theorem 2. Thus, we can view \hat{s}_k as a function $\hat{s}_k(\hat{s}_{k-1}, s_k, \Delta\tilde{\mu}_k, \theta_{0,k})$. Based on [5], we can further derive that

$$\theta_{0,k} \stackrel{(a)}{=} \theta_{k|k-1} \stackrel{(b)}{\approx} \hat{\theta}_{k-1} - \frac{\hat{v}_{k-1} \sin \hat{\theta}_{k-1} T}{\sqrt{x_{k-1}^2 + y_{k-1}^2}}, \quad (22)$$

where $\theta_{k|k-1}$ is the predicted AoD at time slot k , given the estimated AoD $\hat{\theta}_{k-1}$ at time slot $k-1$. Specifically, (a) in (22) captures the principle of beam tracking, whereby the beam direction $\theta_{0,k}$ at time slot k is determined based on the previously estimated AoD of the VU at time slot $k-1$. Moreover, term (b) in (22) is derived based on geometric relationships, under the assumption that the duration of a single time slot is sufficiently short [5], [21], [22]. As a result, we can view $\theta_{0,k}$ as a function $\theta_{0,k}(\hat{s}_{k-1})$. Now we can rewrite $\hat{s}_k(\hat{s}_{k-1}, s_k, \Delta\tilde{\mu}_k, \theta_{0,k})$ as $\hat{s}_k(\xi_k, \Delta\tilde{\mu}_k)$. Finally, we can conclude that the process satisfies the first-order Markov property since $\xi_{k+1} = [\hat{s}_k, s_{k+1}] = [\hat{s}_k(\xi_k, \Delta\tilde{\mu}_k), s_{k+1}]$ and s_k , determined only by the VU, is independent of all past states and actions in the process.

Next, we map problem (21) into an MDP $\mathcal{M} = \{\Xi, \mathcal{A}, \mathcal{P}, R, \gamma\}$, where Ξ is the state space, \mathcal{A} is the action space, $\mathcal{P} : \Xi \times \Xi \times \mathcal{A} \rightarrow \mathbb{R}$ is the stochastic state transition function, $R : \Xi \times \mathcal{A} \rightarrow \mathbb{R}$ is the reward function, and γ is the discount factor for future reward. The components of \mathcal{M} is detailed as the following:

- **Agent:** The agent is the attacker that controls the malicious RIS.
- **Action:** According to Theorem (1) and analysis in Section III, the action at time slot k is defined as the spoofing frequency, i.e., $\Delta\tilde{\mu}_k \in \mathcal{A}_k \subset \mathcal{A}$. In other words, the actual action space \mathcal{A}_k at time slot k is a subspace of \mathcal{A} , which varies across different time slots.
- **States:** The state ξ_k at time slot k is the spoofed sensing outcome \hat{s}_{k-1} at last time slot $k-1$ and the true state s_k of VU at time slot k , i.e., $\xi_k = [\hat{s}_{k-1}, s_k] \in \Xi$.
- **Reward:** The reward assigned to the agent at time slot k must reflect how well the spoofed sensing outcome \hat{s}_k satisfies the spatial and temporal consistency with respect to \hat{s}_{k-1} . Thus, we define $R(\xi_k, \Delta\tilde{\mu}_k) = \sum_i \min(0, c_i(\hat{s}_{k-1}, \hat{s}_k))$, where $c_i(\hat{s}_{k-1}, \hat{s}_k)$ is the i -th element in $c(\hat{s}_{k-1}, \hat{s}_k)$ ³. Specifically, when $c_i(\hat{s}_{k-1}, \hat{s}_k) \geq 0$ for $\forall i$ is satisfied, the reward is maximized as $R(\xi_k, \Delta\tilde{\mu}_k) = 0$, which captures the condition that the spoofed sensing outcome satisfies the spatial and temporal consistency and is difficult to distinguish from regular and real-world trajectories.

To solve the sequential decision-making problem in \mathcal{M} , we can use any off-the-shelf RL framework to find the policy π that maximizes the expected discounted reward $J = \mathbb{E}_\pi [\sum_{k=0}^{\infty} \gamma^k R(\xi_k, \Delta\tilde{\mu}_k)]$. However, one challenge here is that the feasible action of \mathcal{M} depends on the specific state. Particularly, Theorem 1 shows that \mathcal{A}_k can be viewed as a function $\mathcal{A}_k(\theta_{0,k}, s_k)$, while other parameters are time-invariant. Since $\theta_{0,k}$ can be viewed as $\theta_{0,k}(\hat{s}_{k-1})$, we can rewrite $\mathcal{A}_k(\theta_{0,k}, s_k)$ as $\mathcal{A}_k(\hat{s}_{k-1}, s_k) = \mathcal{A}_k(\xi_k)$, i.e., the feasible action set of \mathcal{M} varies with its current state. To discard the infeasible actions, we next incorporate a popular RL technique named action mask [27].

To use action mask, we first discretize $\mathcal{A} = [0, \frac{1}{\Delta T}]$ into L discrete actions as $\hat{\mathcal{A}} = \{\Delta\mu, \dots, L\Delta\mu\}$ with the discretiza-

³The reward $R(\xi_k, \Delta\tilde{\mu}_k)$ is accessible to the RIS as both \hat{s}_{k-1} and \hat{s}_k can be derived by the RIS through Theorems 1 and 2.

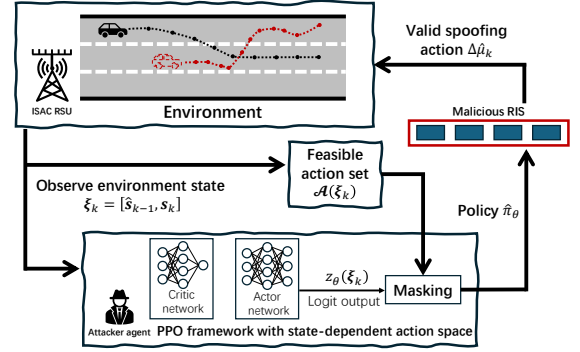


Fig. 3. The PPO framework with action mask for spoofing the trajectory of VU.

tion step $\Delta\mu = \frac{1}{\Delta T L}$. As a result, we obtain a MDP of discrete action space and continuous state space. The standard PPO framework is selected for solving the MDP, as it supports discrete action spaces and ensures stable training through clipped policy updates. Moreover, as a policy-based RL framework, PPO directly outputs the probabilities of selecting certain actions, which can be seamlessly integrated with the action masking mechanism to satisfy the state-dependent action constraints (21b). Specifically, we seek to train a policy network of vector output $z_\theta(\xi) = [z_1(\xi), \dots, z_L(\xi)] \in \mathbb{R}^L$, where $z_l(\xi)$ represents the raw logit output for action $l\Delta\mu$ given state ξ . We adopt the standard PPO training procedure as described in [28] and focus on the integration of the action mask mechanism. Typically, the policy in standard PPO is derived by applying a softmax over the vector output $z_\theta(\xi)$, as follows:

$$\pi_\theta(l\Delta\mu | \xi) = \frac{\exp(z_l(\xi))}{\sum_{l'=1}^L \exp(z_{l'}(\xi))}, \quad (23)$$

which is essentially the probability of selecting $\Delta\tilde{\mu} = l\Delta\mu$ given state ξ . Due to the state-dependent action, we aim to modify the probability of selecting invalid actions to zero. To this end, the action mask mechanism adjusts the logit output $z_l(\xi)$ as following:

$$\tilde{z}_l(\xi) = z_l(\xi) + \log(\alpha + (1 - \alpha)m_l(\xi)), \quad (24)$$

where $\alpha \in (0, 1)$ is a small positive constant (e.g., 0.01) and $m_l(\xi)$ is the binary action mask defined as

$$m_l(\xi) = \begin{cases} 1, & l\Delta\mu \in \mathcal{A}(\xi), \\ 0, & l\Delta\mu \notin \mathcal{A}(\xi). \end{cases} \quad (25)$$

Subsequently, the masked policy is redefined as

$$\hat{\pi}_\theta(l\Delta\mu | \xi) = \frac{\exp(\tilde{z}_l(\xi))}{\sum_{l'=1}^L \exp(\tilde{z}_{l'}(\xi))}. \quad (26)$$

Based on (24), (25), and (26), we can observe that the masked policy assigns lower probabilities to invalid actions, reducing their likelihood of being selected to near zero. Given the modified policy in (26), the influence of the binary action mask $\mathbf{m}(\xi) = [m_1(\xi), \dots, m_L(\xi)]$ remains differentiable, thereby ensuring faster and more stable convergence of the PPO training process and a valid sensing spoofing in our scenario. The overall PPO framework with action mask is shown in Fig. 3.

In presence of trajectory-level sensing spoofing, it is challenging to identify spoofed trajectories via typical deep

clustering-based detection method [29], which extracts the latent representation of a given trajectory. By measuring the distance between the obtained representation and the cluster center of regular trajectories' representations, the spoofed trajectories can be identified. However, since the spoofed trajectory induced by (21) still follows the consistency constraints, its latent representation may not be separable from those of regular trajectories. To address this issue, we observe that real-world trajectories generally exhibit certain intentions (e.g., lane changing), which are difficult for an attacker to imitate under (21b). Thus, we next propose an STL-based attack detection framework which learns interpretable formulas that characterize how regular trajectory evolves over time according to typical driving intentions.

V. STL-BASED ATTACK DETECTION FRAMEWORK

In this section, from a defender's perspective, we design an attack detection framework at the RSU. Specifically, we incorporate a neuro-symbolic structure named TLINet [20] to learn the STL formulas for identifying spoofed trajectories.

A. STL Preliminaries

Briefly, STL is a formal language expressing the complex temporal and logical properties of a signal sequence. Through a series of structural operators, STL can quantify how well a signal sequence satisfies some desired objectives. Here we only consider a simplified STL without the until operator [30]. The syntax and semantics of STL are defined as follows:

Definition 1. For a trajectory $\mathcal{S} = [s_1, \dots, s_K]$ over K time slots, the syntax of the corresponding STL formulas is defined recursively as:

$$\phi ::= \mu \mid \phi_1 \wedge \phi_2 \mid \phi_1 \vee \phi_2 \mid \Diamond_{[k_1, k_2]} \phi \mid \Box_{[k_1, k_2]} \phi, \quad (27)$$

where $\mu := f_\mu(s_k) \geq 0$ is a Boolean predicate with $f_\mu : \mathbb{R}^d \rightarrow \mathbb{R}$. ϕ, ϕ_1, ϕ_2 are STL formulas. The Boolean operators \wedge, \vee are conjunction and disjunction, respectively. The temporal operators \Diamond, \Box represent "eventually" and "always". Let $0 \leq k_1 \leq k_2 \leq K$ and $k_1, k_2 \in \mathbb{Z}$, $\Diamond_{[k_1, k_2]} \phi$ is true if ϕ is satisfied for at least one point $k \in [k_1, k_2] \cap \mathbb{Z}$, while $\Box_{[k_1, k_2]} \phi$ is true if ϕ is satisfied for all time points $k \in [k_1, k_2] \cap \mathbb{Z}$.

Definition 1 provides a formal way to describe the temporal and logical properties of a trajectory \mathcal{S} . Compared with the simple consistency requirement (e.g., (20)), such STL formulas capture the inherent temporal patterns of \mathcal{S} , providing a more semantic and interpretable perspective in identifying whether a certain trajectory is spoofed. To quantify how well a trajectory \mathcal{S} satisfies the STL formula ϕ , the quantitative semantics of ϕ , also called the STL robustness, is defined next.

Definition 2. The quantitative semantics of an STL formula ϕ for s_k are defined as:

$$r(s_k, \mu) = f_\mu(s_k), \quad (28)$$

$$r(s_k, \wedge_{i=1}^n \phi_i) = -\max_{i=1, \dots, n} [-r(s_k, \phi_i)], \quad (29)$$

$$r(s_k, \vee_{i=1}^n \phi_i) = \max_{i=1, \dots, n} r(s_k, \phi_i), \quad (30)$$

$$r(s_k, \Box_{[k_1, k_2]} \phi) = -\max_{k' \in [k+1, k+k_2]} [-r(s_{k'}, \phi)], \quad (31)$$

$$r(s_k, \Diamond_{[k_1, k_2]} \phi) = \max_{k' \in [k+1, k+k_2]} r(s_{k'}, \phi). \quad (32)$$

With Definition 2, a trajectory \mathcal{S} is said to satisfy ϕ , i.e., $\mathcal{S} \models \phi$, if and only if $r(s_0, \phi) \geq 0$. Otherwise, \mathcal{S} is said to violate ϕ , i.e., $\mathcal{S} \not\models \phi$ with $r(s_0, \phi) < 0$. For example, if $r(s_k, \mu) \geq 0$, we can conclude from (28) that the Boolean predicate $\mu := f_\mu(s_k) \geq 0$ is true since $r(s_k, \mu) = f_\mu(s_k) \geq 0$. Similarly, for (29), if $r(s_k, \wedge_{i=1}^n \phi_i) = -\max_{i=1, \dots, n} [-r(s_k, \phi_i)] \geq 0$, we can derive that $r(s_k, \phi_i) \geq 0, \forall i = 1, \dots, n$, which means s_k satisfies all the formulas ϕ_1, \dots, ϕ_n , i.e., $\wedge_{i=1}^n \phi_i$. The rest quantitative semantics (30) - (32) can be explained in a similar way. Given Definitions 1 and 2, STL formulas can be used by the RSU to determine whether the sensed trajectory $\hat{\mathcal{S}}$ satisfies certain properties, thereby enabling the detection of potential RIS spoofing attacks.

Our goal is to learn an STL formula ϕ that can accurately distinguish fake trajectories from regular, real-world trajectories, which is essentially an STL formula inference problem [31]. Specifically, assume that we have a labeled trajectory dataset $\mathcal{D} = \{(\mathcal{S}_1, c_1), \dots, (\mathcal{S}_D, c_D)\}$ with $c_d = 1$ indicating normal trajectory \mathcal{S}_d collected without spoofing while $c_d = 0$ indicating abnormal trajectory \mathcal{S}_d collected under spoofing. Then, the objective is to learn both structure and parameters (such as k_1, k_2 , and $f_\mu(\cdot)$) of ϕ to minimize the misclassification rate $\frac{1}{D} |\{ \mathcal{S}_d \mid (\mathcal{S}_d \models \phi \wedge c_d = 1) \vee (\mathcal{S}_d \not\models \phi \wedge c_d = 0) \}|$. Such an STL-based attack detection framework can be easily deployed, as it only requires a dataset of vehicle trajectories collected by the RSU. These data can be practically obtained via the RSU's sensing functionality and used to learn the STL formulas offline, independently of the detection phase. Finally, the learned formula ϕ can identify RIS spoofing attack once $r(\hat{s}_0, \phi) < 0$ is detected for a sensed trajectory $\hat{\mathcal{S}}$.

B. Clustering of One-class Dataset

However, in practice, it is challenging to obtain a labeled data set \mathcal{D} that includes enough spoofed outcomes with $c_d = 0$ because of two reasons: (i) It is easy to obtain normal trajectory since all sensing outcomes collected without spoofing can be defined as normal, while abnormal trajectory is hard to define; (ii) The samples of abnormal trajectories collected under attacks are comparatively limited. Thus, we are faced with a one-class anomaly detection problem [29] where we need to classify normal and abnormal trajectories, while only trajectories labeled as normal are available.

To address this challenge, we propose a self-supervised framework. Specifically, our approach, inspired by pseudo-labeling methods [32], first clusters the unlabeled dataset \mathcal{D} into P behavioral categories. For each identified type p , a one-vs-rest attack detector is trained based on a new dataset \mathcal{D}_p . The trajectory \mathcal{S}_d in \mathcal{D}_p is labeled as "in-class" ($c_d = 1$) if it belongs to the cluster p , and "out-of-class" ($c_d = 0$) otherwise, serving as pseudo-labels for learning a one-vs-rest attack detector. Subsequently, an STL formula ϕ_p is learned to characterize the temporal logic pattern for type p and P STL formulas ϕ_1, \dots, ϕ_P will be obtained in total. During deployment, the RSU first classifies $\hat{\mathcal{S}}$ into one of the predefined types, e.g., p . Then, the corresponding learned STL formula ϕ_p is used to verify the consistency of $\hat{\mathcal{S}}$ through its robustness $r(\hat{s}_0, \phi_p)$. Given $\hat{\mathcal{S}}$, sensing attack is detected when

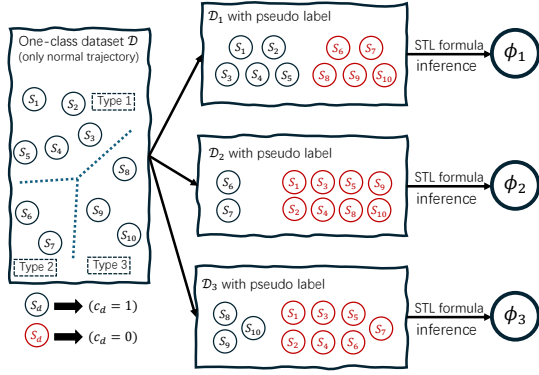


Fig. 4. The illustration of clustering a one-class dataset into P pseudo-labeled datasets.

$S_d \notin \phi$, i.e., $r(\hat{s}_0, \phi_p) < 0$. The overall pipeline for generating multiple one-vs-rest training datasets is illustrated in Fig. 4.

In the proposed framework, we incorporate deep temporal clustering representation (DTCR) [33] to cluster the spatial temporal trajectories in dataset \mathcal{D} . Specifically, DTCR clusters unlabeled data into multiple categories based on their latent representations. Different from the two-stage approaches that independently extracts latent features and then clusters, DTCR jointly optimizes these two process. In short, the latent representations are not only learned for accurate reconstruction, but also for an effective clustering. The construction of P one-vs-rest datasets consists of two components: a) an autoencoder that learns the latent representation of the given trajectory, and b) a K-means clustering algorithm to guide the latent representation learning.

1) *Representation Learning*: For the representation learning, we aim to train an encoder $f_{\text{En}}(\cdot) : \mathbb{R}^{d \times K} \rightarrow \mathbb{R}^m$ that maps the trajectory S_d into latent representations, where m is the dimension of the latent space. The learned representation $h_d = f_{\text{En}}(S_d)$ should be able to reconstruct the input trajectory through a paired decoder $f_{\text{De}}(\cdot) : \mathbb{R}^m \rightarrow \mathbb{R}^{d \times K}$. Specifically, parameterized $f_{\text{En}}(\cdot)$ and $f_{\text{De}}(\cdot)$ should be trained to minimize the reconstruction loss $L_{\text{re}} = \frac{1}{D} \sum_{d=1}^D \|f_{\text{De}}(h_d) - S_d\|^2$. However, the learned representation may be restricted to the reconstruction task if only the reconstruction loss is considered. To facilitate the latent representation h_d a good clustering performance, features distinct for clustering should be incorporated.

2) *K-means Clustering*: Given the latent representation matrix $H = [h_1, \dots, h_D] \in \mathbb{R}^{M \times D}$, the standard K-means clustering objective can be equivalently reformulated, following [34], as finding discrete cluster indicator matrix $F \in \mathbb{R}^{D \times P}$ to minimize $L_{\text{cl}} = \text{Tr}(H^T H) - \text{Tr}(F^T H^T H F)$. The d -th row of F indicates the cluster membership of trajectory S_d . Since optimizing a discrete indicator matrix F is NP-hard, a common relaxation is to drop the discrete constraint and instead require F to satisfy the orthogonality condition $F^T F = I$. The closed-form solution of F can be then obtained by composing the first P singular vectors of H according to the Ky Fan theorem [33]. Finally, to obtain discrete cluster labels, K-means clustering is applied to the row vectors of the relaxed matrix F , i.e., a more cluster-friendly representation of H , for clustering the trajectories in \mathcal{D} .

Algorithm 1 Clustering of the one-class dataset

Require: One-class dataset \mathcal{D} , number of clusters P , iteration round i_{max} , and update round i_{T}
Ensure: Encoder $f_{\text{En}}(\cdot)$, decoder $f_{\text{De}}(\cdot)$, P cluster centers $\delta_1, \dots, \delta_P$, and P pseudo-labeled datasets $\mathcal{D}_1, \dots, \mathcal{D}_P$

- 1: Initialize $f_{\text{En}}(\cdot)$ and $f_{\text{De}}(\cdot)$ with random parameters.
- 2: Derive F based on the representation matrix H given by the initial encoder $f_{\text{En}}(\cdot)$.
- 3: **for** $i = 1$ to i_{max} **do**
- 4: With derived F , update the parameters of $f_{\text{En}}(\cdot)$ and $f_{\text{De}}(\cdot)$ according to the loss given in (33a)
- 5: **if** $i \% i_{\text{T}} = 0$ **then**
- 6: With derived H , update F according to Ky Fan theorem.
- 7: **end if**
- 8: **end for**
- 9: Apply K-means clustering to F for obtaining the cluster membership of trajectories in \mathcal{D} and P cluster centers $\delta_1, \dots, \delta_P$.
- 10: **for** $p = 1$ to P **do**
- 11: Label all the “in-class” trajectories S_d in \mathcal{D} clustered as type p with $c_d = 1$, while the remaining “out-of-class” trajectories with $c_d = 0$.
- 12: Construct \mathcal{D}_p with pseudo labels.
- 13: **end for**

3) *Joint Training*: Recall that our aim is to learn H that simultaneously captures essential features for reconstruction and preserves discriminative structures for effective clustering. Thus, the joint training considering both reconstruction loss L_{re} and the clustering loss L_{cl} to optimize $f_{\text{En}}(\cdot)$ and $f_{\text{De}}(\cdot)$ can be formulated as follows:

$$\min_{F, H} L_{\text{joint}} = L_{\text{re}} + \lambda_0 L_{\text{cl}} \quad (33a)$$

$$\text{s.t. } F^T F = I, \quad (33b)$$

where λ_0 is the regularization parameter. Given fixed F , the joint objective (33) can be optimized with respect to the parameters of $f_{\text{En}}(\cdot)$ and $f_{\text{De}}(\cdot)$ via gradient backpropagation. Therefore, we adopt an alternating optimization strategy, where F and the parameters of $f_{\text{En}}(\cdot)$ and $f_{\text{De}}(\cdot)$ are updated iteratively. The overall training procedure of the clustering is summarized in Algorithm 1.

C. Neuro-symbolic Learning of STL Formulas

After constructing P one-vs-rest labeled datasets, we train an attack detection model for each dataset \mathcal{D}_p . The objective is to infer an STL formula ϕ_p that characterizes the normal behavior for type p , and subsequently identifies spoofed trajectory. To this end, we incorporate a novel neuro-symbolic framework named TLINet [20] composed of three differentiable layers. Each layer is designed to capture one unique property of the trajectory, which is detailed as follows:

1) *Predicate Layer*: A predict layer is composed of multiple independent predicate modules. Each predicate module takes trajectory S as input and outputs the robustness vector $r(S, \mu) = [r(s_1, \mu), \dots, r(s_K, \mu)]$ over a predicate μ . The predicate module captures general low-level properties of trajectories, such as position or speed constraints, that hold across the entire time horizon. Similar to [31] and [20], we consider a simplified linear predicate $f_{\mu}(s_k) = a^T s_k - b$, where $a \in \mathbb{R}^d$ and $b \in \mathbb{R}$ are the parameters to be learned. The structure of predicate layer is shown in Fig. 5a.

2) *Boolean Layer*: A Boolean layer is also composed of multiple dependent Boolean modules. However, a single Boolean module will take the robustness vectors

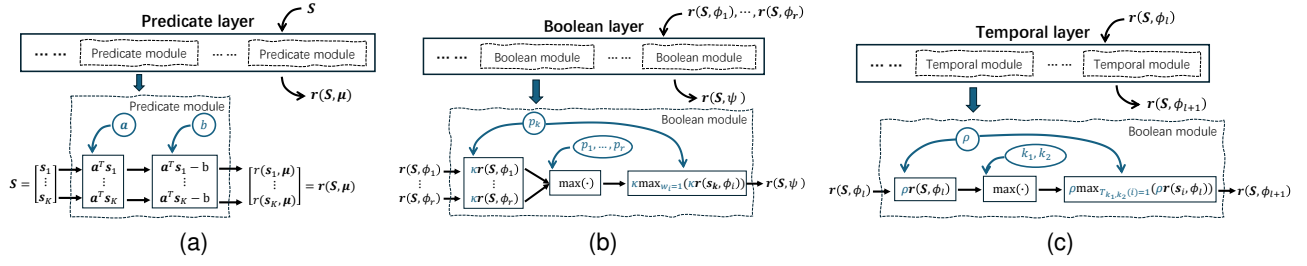


Fig. 5. Three basic differentiable layers in TLINet: a) Predicate layer, b) Boolean layer, c) Temporal layer. The trainable parameters are denoted in blue.

$\mathbf{r}(\mathbf{S}, \phi_1), \dots, \mathbf{r}(\mathbf{S}, \phi_r)$ of a series of sub-formulas ϕ_1, \dots, ϕ_r as input and outputs $\mathbf{r}(\mathbf{S}, \psi)$ with $\psi = \bigwedge_{i=1}^r \phi_r \mid \bigvee_{i=1}^r \phi_r$. Essentially, the Boolean layer can encode the conjunction and disjunction operation defined in (29) and (30), and, thus, the model can now combine multiple low-level predicates. Such integration enables the system to identify spoofed trajectory over combinations of features, e.g., detecting abnormal patterns when multiple spatial constraints are jointly violated. The structure of Boolean layer is illustrated in Fig. 5b. To unify the discrete selection between logical operations $\bigwedge_{i=1}^r \phi_r$ and $\bigvee_{i=1}^r \phi_r$, a learnable selection operator $\kappa \sim \text{Ber}_{\text{ML}, \mathcal{X}_\kappa}(p_\kappa)$ with $\mathcal{X} = \{1, -1\}$ is incorporated. Specifically, the operation of $\bigwedge_{i=1}^r \phi_r$ and $\bigvee_{i=1}^r \phi_r$ on s_k can be unified as $\kappa \max_i(\kappa r(s_k, \phi_i))$ according to (29) and (30). Moreover, $\text{Ber}_{\text{ML}, \mathcal{X}}(p)$ with $\mathcal{X} = \{X_0, X_1\}$ is the *maximum likelihood draw* distribution and $x \sim \text{Ber}_{\text{ML}, \mathcal{X}}(p)$ indicates that

$$\begin{aligned} P(x = X_0) &= 1, & \text{if } 0.5 \leq p \leq 1, \\ P(x = X_1) &= 1, & \text{if } 0 \leq p < 0.5. \end{aligned} \quad (34)$$

Thus, the discrete selection between different operations can be learned via the training update of parameter p_κ . When $0.5 \leq p_\kappa \leq 1$ is learned, then the operator is $\kappa = 1$, which represents the disjunction operation. Similarly, we define $\mathbf{w} = [w_1, \dots, w_r]$ with $w_i \sim \text{Ber}_{\text{ML}, \mathcal{X}_w}(p_i)$, $\forall i = 1, \dots, r$ and $\mathcal{X}_w = \{0, 1\}$ to guide the participation of sub-formulas ϕ_1, \dots, ϕ_r in Boolean operation. Thus, ϕ_r will only be included in the Boolean composition if $w_r = 1$, allowing the network to selectively compose sub-formulas via the training update of parameters p_1, \dots, p_r . The k -th element of $\mathbf{r}(\mathbf{S}, \psi)$ is calculated as $r(s_k, \psi) = \kappa \max_{w_i=1}(\kappa r(s_k, \phi_i))$. Finally, the trainable parameters of a Boolean layer are p_κ and p_1, \dots, p_r . Moreover, to facilitate a differentiable max operation, the averaged max approximation [20] is incorporated.

3) *Temporal Layer*: The temporal layer is composed of multiple temporal module. Each temporal module takes $\mathbf{r}(\mathbf{S}, \phi_l)$ of a lower-level formula ϕ_l as input and outputs $\mathbf{r}(\mathbf{S}, \phi_{l+1})$ of a higher-level formula ϕ_{l+1} by applying a temporal operator \diamond or \square over a specified time interval $[k_1, k_2]$ on ϕ_l . In other words, temporal layer can encode nested temporal operation $\phi_{l+1} = \diamond_{[k_1, k_2]} \phi_l \mid \square_{[k_1, k_2]} \phi_l$. This layer allows the model to identify persistent or transient violations of expected behaviors across time. For instance, trajectories with repeated violations of a given predicate over multiple time steps are generally more indicative of spoofing. Thus, the temporal layer enables the system to capture long-range temporal consistency in the trajectory of a VU. Similarly, a learnable selection operator $\rho \sim \text{Ber}_{\text{ML}, \mathcal{X}_\rho}(p_\rho)$ with $\mathcal{X}_\rho = \{1, -1\}$ is used in the temporal layer to determine different logical operations $\diamond_{[k_1, k_2]} \phi_l$ and $\square_{[k_1, k_2]} \phi_l$ ((31) and (32)). To facilitate the

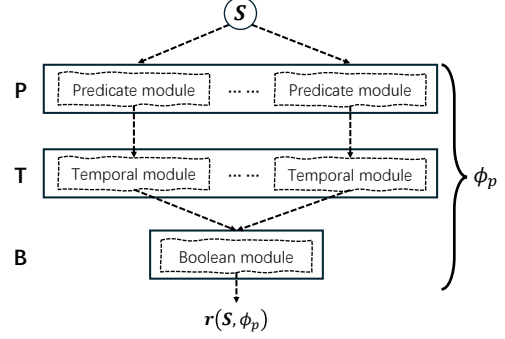


Fig. 6. An illustrative example of TLINet composed of one predicate layer, one temporal layer, and one Boolean layers.

training of the time interval $[k_1, k_2]$, a trainable time vector $T_{k_1, k_2} = [i_0, \dots, i_{K-1}] \in \{0, 1\}^K$ is incorporated:

$$\begin{aligned} T_{k_1, k_2} &= \frac{1}{\eta} \min(\text{ReLU}(\mathbf{n} - \mathbf{1}(k_1 - \eta)) - \text{ReLU}(\mathbf{n} - \mathbf{1}k_1)) \\ &\quad \times \text{ReLU}(-\mathbf{n} + \mathbf{1}(k_2 + \eta)) - \text{ReLU}(-\mathbf{n} + \mathbf{1}k_2)), \end{aligned} \quad (35)$$

where $\mathbf{n} = [0, 1, \dots, k-1]$, $\mathbf{1}$ is a all one vector, and η is a positive hyperparameter controlling the slope steepness of T_{k_1, k_2} . T_{k_1, k_2} acts as an indicator vector such that $T_{k_1, k_2}(k) = 1, k_1 \leq k \leq k_2$ and $T_{k_1, k_2}(k) = 0, k < k_1 \vee k > k_2$. Consequently, the temporal operators $\diamond_{[k_1, k_2]} \phi_l$ and $\square_{[k_1, k_2]} \phi_l$ operate exclusively over time steps with indicator vector T_{k_1, k_2} equal to 1, restricting their scope to the interval $k_1 \leq k \leq k_2$. Element k of $\mathbf{r}(\mathbf{S}, \phi_{l+1})$ is calculated as $r(s_k, \phi_{l+1}) = \rho \max_{T_{k_1, k_2}(i)=1}(\rho r(s_i, \phi_l))$. The trainable parameters of the Boolean module are p_ρ and k_1, k_2 , as shown in Fig. 5c. Similarly, the differentiable max operation is realized by the sparse softmax proposed in [20].

By flexibly stacking temporal or Boolean layers on top of the predicate layer, we can construct TLINet to learn the STL formula ϕ_p for each dataset \mathcal{D}_p . A representative illustration is given in Fig. 6. Here, the predicate layer, serving as the foundation, learns basic predicate of the trajectory's features. Then, a temporal layer is stacked to formulate the temporal relationship of the trajectory. Finally, a Boolean layer is used to decide the conjunction or disjunction logic and output the robustness value of the given trajectory. For the training process of the STL formula, a composite loss function incorporating task-specific objectives and regularization terms is adopted. Take ϕ_p for instance, the total loss is given by

$$L_{\text{STL}} = \mathcal{L}_{\text{task}} + \lambda_1 \mathcal{L}_s + \lambda_2 \mathcal{L}_{\text{avm}} + \lambda_3 \mathcal{L}_{\text{kavm}}, \quad (36)$$

where $\mathcal{L}_{\text{task}} = \frac{1}{D} \sum_{d=1}^D e^{-cd r(s_d, 0, \phi_p)}$ is the main task loss for classifying “in-class” and “out-of-class” samples, $\lambda_1, \lambda_2, \lambda_3 \in \mathbb{R}_+$ are balancing coefficients, and $\mathcal{L}_s, \mathcal{L}_{\text{avm}}, \mathcal{L}_{\text{kavm}}$ are

Algorithm 2 STL-based attack detection

Require: Sensing outcome $\hat{\mathcal{S}}$ (trajectory), well-trained encoder $f_{\text{En}}(\cdot)$, P STL formulas ϕ_1, \dots, ϕ_P , and P cluster centers $\delta_1, \dots, \delta_P$.

Ensure: Spoofing detection result for $\hat{\mathcal{S}}$.

- 1: Obtain the latent representation of the sensing outcome $\hat{\mathbf{h}} = f_{\text{En}}(\hat{\mathcal{S}})$.
 - 2: Derive the distance between $\hat{\mathbf{h}}$ and cluster center $d_p = \|\hat{\mathbf{h}} - \delta_p\|_2$ and cluster $\hat{\mathcal{S}}$ into type $p^* = \arg \min_p d_p$.
 - 3: Identify spoofed trajectory if $r(\hat{\mathbf{s}}_0, \phi_{p^*}) < 0$.
-

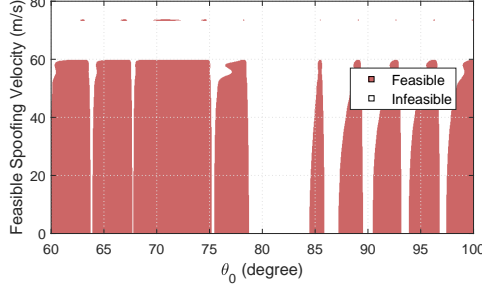


Fig. 7. Feasible spoofing velocity versus beam steering direction.

auxiliary regularization losses. In particular, \mathcal{L}_s encourages the sparsity in the learned structure of ϕ_p , \mathcal{L}_{avm} serves as the regularizer to promote distinct sub-formula selection in the Boolean layer, and $\mathcal{L}_{\text{kavm}}$ stabilizes choice between different logical operations when applying differentiable logical aggregation. The detailed formulation of each regularization term can be found in [20]. Finally, the STL-based attack detection framework is given in Algorithm 2. In summary, the proposed STL-based detection framework yields interpretable formulas that enable explicit inference of spoofing attack, while also providing structural transparency of the detection method in safety-critical ISAC systems.

VI. SIMULATION RESULTS AND ANALYSIS

For our simulations, we consider a two-dimensional Cartesian coordinate system with the RSU located at its origin. The RIS is fixed at $(x_R, y_R) = (5 \text{ m}, 15 \text{ m})$, i.e., $\theta_R = 71.6^\circ$. The parameters of the ISAC vehicular network are set as follows unless specified otherwise later: $P = 30 \text{ dBm}$, $\sigma^2 = -100 \text{ dBm}$, $f_c = 28 \text{ GHz}$, $N_t = N_r = 32$, $M = 32$, $\kappa_V = 7 \text{ dBsm}$, $\eta = 0.8$, $S = 50 \text{ cm} \times 10 \text{ cm}$, $T = 10 \text{ ms}$, and $\Delta T = 1 \text{ ms}$ [5], [22], [26]. The parameters for the consistency constraints are $a_{\max} = 3 \text{ m/s}^2$, $a_{\min} = -3 \text{ m/s}^2$, $\delta_x = 1 \text{ m}$, and $\delta_y = 0.3 \text{ m}$. The hyperparameters for the clustering Algorithm 1 are $i_{\max} = 50$ and $i_T = 5$.

We first examine the impact of the malicious RIS on the sensing outcomes in a single time slot. The coordinates of the VU in the considered slot are assumed as $(x_V, y_V) = (3 \text{ m}, 21 \text{ m})$, i.e., $\theta_V = 81.9^\circ$. Moreover, we assume $v = 10 \text{ m/s}$, and, thus, the Doppler shift can be derived as $\mu_V = v f_c \cos \theta_V$. Fig. 7 shows the impact of RIS spoofing on the estimated velocity of the VU, which can be derived by the spoofed Doppler shift. In particular, the different feasible spoofing velocity sets, derived from (13), versus the RSU's beam steering direction θ_0 are illustrated. From Fig. 7, we can observe that, generally, a beam steered in the proximity of the VU's direction ($\theta_V = 81.9^\circ$) can eliminate the impact of RIS spoofing. For instance, when $\theta_0 \in (78^\circ, 84^\circ)$, we

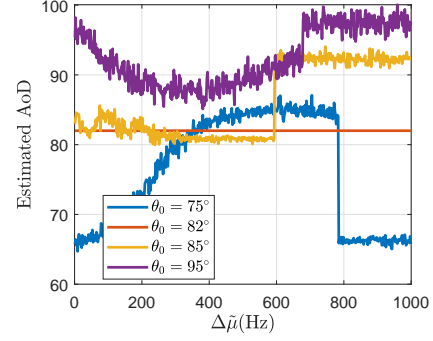


Fig. 8. Impact of Doppler shift spoofing on the resulted MLE of AoD.

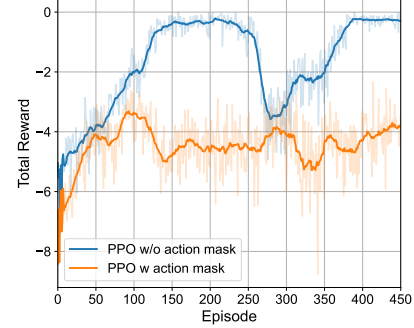


Fig. 9. Reward versus PPO training episodes.

have $\mathcal{A} = \emptyset$, indicating that no successful spoofing can be conducted. However, when θ_0 is slightly misaligned with the VU, e.g., $\theta_0 = 77^\circ$ (a deviation of -4.9°) or $\theta_0 = 85^\circ$ (a deviation of 3.1°), the RSU may obtain a spoofed velocity ranging from 0.1 m/s to 60 m/s , introducing a significant estimation error of -9.9 m/s to 50 m/s with respect to the true velocity $v = 10 \text{ m/s}$.

In Fig. 8, we show the spoofed MLE for the AoD as a function of the spoofing frequency on the Doppler shift estimation. The estimated values for the AoD are averaged over 200 trials of independent noise. First, we can observe that the MLE for the AoD will not be affected under a beam perfectly steered to the VU when $\theta_0 = 82^\circ$. However, the RIS can always find a spoofing frequency that causes a severe deviation of the spoofed MLE under beam misalignment. For instance, when $\theta_0 = 85^\circ$ deviates by only 3.1° from θ_V , its MLE can be spoofed as 92° with $\Delta \tilde{\mu} \geq 600 \text{ Hz}$, leading to an estimation error of at least 11° . When $\theta_0 = 75^\circ$ or $\theta_0 = 95^\circ$ is set, the accuracy of AoD estimation is even more significantly compromised.

In Fig. 9, the average reward of the action mask enhanced PPO framework is evaluated and compared to the standard PPO framework (without action mask). From Fig. 9, we can observe that the PPO framework with action mask, though more stable, counterintuitively achieves lower reward after 400 episodes of training, which seemingly indicates that the action mask mechanism hinders the RIS from generating plausible trajectories. However, this observation is misleading and action mask mechanism is actually necessary. Specifically, the PPO framework without action mask tends to choose a spoofing frequency whereby $\Delta \tilde{\mu}_k \notin \mathcal{A}_k$, which naturally satisfies the consistency with higher reward and fails to conduct sensing attack (see Theorem 1). Only with the guarantee provided by

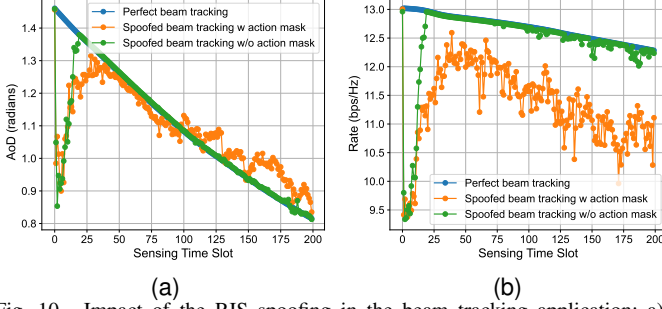


Fig. 10. Impact of the RIS spoofing in the beam tracking application: a) Estimated AoD, b) Communication rate.

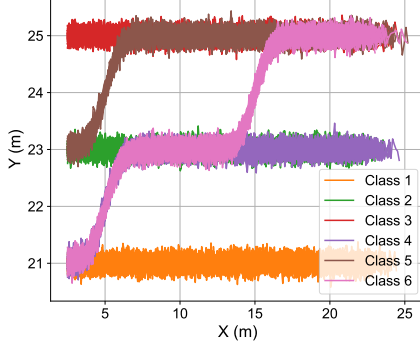


Fig. 11. Clustering results of the trajectory dataset.

action mask mechanism, the invalid spoofing frequencies can be discarded in the PPO framework. As a result, the sensing outcomes of the VU will largely deviate from the ground truth, as shown next in an SAC use case.

To illustrate the impact of the RIS sensing spoofing, we consider the beam tracking application studied in [5]. Specifically, the estimated AoD and achievable rate of the VU are evaluated in Fig. 10a and Fig. 10b. Two beam-tracking strategies are considered. Perfect beam tracking represents the scenario in which the RSU can obtain an accurate sensing outcomes of the VU without the sensing attack, while the spoofed beam tracking represents the scenario under RIS spoofing attack. Two PPO strategies trained with and without action mask are used to determine the spoofing frequency. From Fig. 10a, we can observe that both strategies induce AoD estimation error up to 0.6 radian during the first 25 slots. This is because the VU is close to the RIS, which leads to a larger feasible frequency set and a less accurate AoD estimation. As the VU moves away, the strategy trained without action mask fails to spoof the AoD estimation while that trained with action mask is still able to result AoD estimation error ranging from -0.1 to 0.13 radian. The impact of this AoD estimation error in beam tracking is shown in 10b. For both two strategies, the VU experiences an achievable rate decrease of up to 28 % compared to that under the perfect beam tracking in the first 25 time slots. Moreover, even after the first 25 time slots, the strategy with action mask can still result an achievable rate decrease from 0.3 bps/Hz to 2.5 bps/Hz.

Next, we evaluate the effectiveness of the proposed STL-based neuro-symbolic attack detection framework. First, to train the DTCR clustering framework, we consider a one-class dataset composed of 480 trajectory samples with trajectory length of 67. By exploiting the DTCR clustering framework

TABLE I
LEARNED STL FORMULAS

Class index	STL formula
1	$\Box_{[30,31]} 0.4111x - 0.3976y + 3.8745 > 0.00$
2	$\Box_{[35,36]} (0.8856x - 0.6263y + 3.5292 > 0.00)$ $\wedge \Diamond_{[0,1]} (-0.4278x + 0.1899y - 3.2133 > 0.00)$
3	$\Box_{[3,29]} 0.2661x + 0.2212y - 6.1891 > 0.00$
4	$\Box_{[2,29]} (0.8741x - 0.4169y + 5.7552 > 0.00)$ $\wedge \Box_{[32,55]} (0.4738x - 0.1150y - 1.3614 > 0.00)$
5	$\Box_{[14,26]} -0.0045x + 0.3247y - 7.9649 > 0.00$
6	$\Box_{[1,15]} (0.2649x - 0.3085y + 5.9170 > 0.00)$ $\wedge \Box_{[5,53]} (-0.7463x + 1.0237y - 10.4846 > 0.00)$

TABLE II
HYPERPARAMETERS FOR TLINET

Class index	λ_1	λ_2	λ_3	λ_0
1	$4e-2$	$5e-0$	$5e-0$	$5e1$
2	$1e-3$	$5e-0$	$5e-0$	$5e1$
3	$1e-1$	$1e1$	$1e1$	$5e1$
4	$1e-3$	$5e-0$	$5e-0$	$5e1$
5	$2e-2$	$5e-0$	$5e-0$	$5e1$
6	$2e-2$	$5e-0$	$5e-0$	$5e1$

given in Algorithm 2, the trajectory samples are clustered into six classes, as shown in Fig. 11. Specifically, classes 1, 2, and 3 represent the straight driving pattern, classes 4 and 5 represent the single lane changing pattern, and class 6 represents the double lane changing pattern. At the same time, six pseudo-labeled datasets are obtained and each of them will be used to learn a STL formula via Algorithm 2. We adopt a TLINet of the same structure as given in Fig. 6. The learned formulas for six classes are given in Table I with the training hyperparameters listed in Table II. To evaluate the clustering framework and the learned formulas, 120 normal trajectory samples and 120 spoofed trajectory samples (generated by the trained PPO framework with action mask) are used for testing. Moreover, a deep clustering-based attack detection method is incorporated as benchmark. Specifically, the considered benchmark extracts the latent representation of a test trajectory and classifies it as spoofed if the representation lies far from the cluster center of regular trajectories in the one-class dataset. The confusion matrices demonstrating the classification performance of the benchmark model and the proposed detection model are given in Fig. 12a and Fig. 12b, respectively, where actual positive and actual negative indicate normal and spoofed trajectory, while predicted positive and negative represent the detection result. From Fig. 12a, we can observe that the benchmark fails to identify the spoofed trajectories generated under consistency constraints (with an accuracy of only 20.83%), indicating that their latent representation are not separable from those of regular trajectories. In contrast, our proposed STL-based method achieves a significantly higher detection accuracy of 74.17%, which is 53.34% higher than that of the deep clustering-based benchmark. Moreover, the learned STL formulas, given in Table I, not only provide interpretability but also offer clear logical rules for distinguishing spoofed trajectories.

VII. CONCLUSION

In this paper, we have studied the feasibility of an RIS spoofing attack in vehicular ISAC network. Specifically, we have analyzed the impact of this spoofing on the Doppler shift and AoD estimation of a VU, from both slot-level and trajectory-level perspectives. The necessary conditions for the RIS to conduct such sensing spoofing are derived. To address

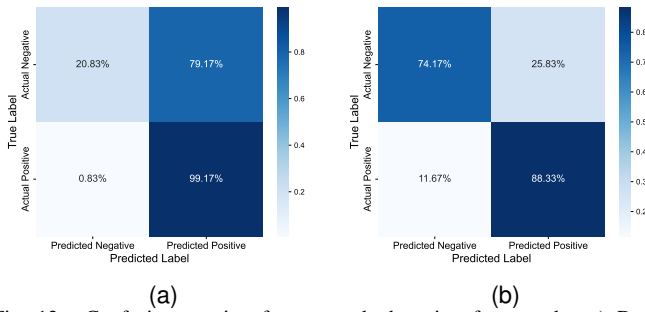


Fig. 12. Confusion matrix of two attack detection frameworks: a) Deep feature-based attack detection, b) Proposed STL-based attack detection.

this attack, we have proposed an STL-based neuro-symbolic attack detection framework, which learns the interoperable formulas for identifying spoofed trajectories. Simulation results showed that the RIS spoofing significantly compromises the sensing accuracy of the RSU. Take the beam tracking application as an example, we have further shown that such sensing estimation error further reduces the VU's achievable rate. Finally, the simulation results show that the proposed STL-based detection framework improves the detection accuracy by 53.34% over the deep clustering-based benchmark, achieving an accuracy of 74.17% in identifying the RIS spoofing.

REFERENCES

- [1] C. Chaccour, W. Saad, M. Debbah, and H. V. Poor, "Joint Sensing, Communication, and AI: A Trifecta for Resilient THz User Experiences," *IEEE Transactions on Wireless Communications*, vol. 23, no. 9, pp. 11 444–11 460, 2024.
- [2] Z. Du, F. Liu, Y. Li, W. Yuan, Y. Cui, Z. Zhang, C. Masouros, and B. Ai, "Toward ISAC-Empowered Vehicular Networks: Framework, Advances, and Opportunities," *IEEE Wireless Communications*, vol. 32, no. 2, pp. 222–229, 2025.
- [3] F. Dong, F. Liu, S. Lu, Y. Xiong, Q. Zhang, Z. Feng, and F. Gao, "Communication-Assisted Sensing in 6G Networks," *IEEE Journal on Selected Areas in Communications*, vol. 43, no. 4, pp. 1371–1386, 2025.
- [4] M. K. Abdel-Aziz, C. Perfecto, S. Samarakoon, M. Bennis, and W. Saad, "Vehicular Cooperative Perception Through Action Branching and Federated Reinforcement Learning," *IEEE Transactions on Communications*, vol. 70, no. 2, pp. 891–903, 2022.
- [5] F. Liu, W. Yuan, C. Masouros, and J. Yuan, "Radar-Assisted Predictive Beamforming for Vehicular Links: Communication Served by Sensing," *IEEE Transactions on Wireless Communications*, vol. 19, no. 11, pp. 7704–7719, 2020.
- [6] Z. Wei, F. Liu, C. Masouros, N. Su, and A. P. Petropulu, "Toward Multi-Functional 6G Wireless Networks: Integrating Sensing, Communication, and Security," *IEEE Communications Magazine*, vol. 60, no. 4, pp. 65–71, 2022.
- [7] N. Su, F. Liu, and C. Masouros, "Secure Radar-Communication Systems With Malicious Targets: Integrating Radar, Communications and Jamming Functionalities," *IEEE Transactions on Wireless Communications*, vol. 20, no. 1, pp. 83–95, 2021.
- [8] N. Su, F. Liu, Z. Wei, Y.-F. Liu, and C. Masouros, "Secure Dual-Functional Radar-Communication Transmission: Exploiting Interference for Resilience Against Target Eavesdropping," *IEEE Transactions on Wireless Communications*, vol. 21, no. 9, pp. 7238–7252, 2022.
- [9] Y. Cao, L. Duan, and R. Zhang, "Sensing for Secure Communication in ISAC: Protocol Design and Beamforming Optimization," *IEEE Transactions on Wireless Communications*, vol. 24, no. 2, pp. 1207–1220, 2025.
- [10] F. Xu, W. Lai, and K. Shen, "Intelligent Surface Assisted Radar Stealth Against Unauthorized ISAC," *IEEE Wireless Communications Letters*, vol. 14, no. 4, pp. 1149–1153, 2025.
- [11] X. Shao and R. Zhang, "Target-Mounted Intelligent Reflecting Surface for Secure Wireless Sensing," *IEEE Transactions on Wireless Communications*, vol. 23, no. 8, pp. 9745–9758, 2024.
- [12] B. Zheng, X. Xiong, J. Tang, and R. Zhang, "Intelligent Reflecting Surface-Aided Electromagnetic Stealth Against Radar Detection," *IEEE Transactions on Signal Processing*, vol. 72, pp. 3438–3452, 2024.
- [13] H. Wang, B. Zheng, X. Shao, and R. Zhang, "Intelligent Reflecting Surface-Aided Radar Spoofing," *IEEE Wireless Communications Letters*, vol. 13, no. 10, pp. 2722–2726, 2024.
- [14] T. Ma, X. Lei, H. Niu, and C. Yuen, "Sensing-Resistant Jamming: A Novel Physical Layer Attack in ISAC Networks," *IEEE Wireless Communications Letters*, vol. 13, no. 11, pp. 3099–3103, 2024.
- [15] H. Huang, H. Zhang, W. Mei, J. Li, Y. Cai, A. L. Swindlehurst, and Z. Han, "Integrated Sensing and Communication Under DISCO Physical-Layer Jamming Attacks," *IEEE Wireless Communications Letters*, vol. 13, no. 11, pp. 3044–3048, 2024.
- [16] A. Guillén, A. Porcel, M. Lazaro Marti, R. Villarino, and D. Girbau, "Spoofing Attacks on FMCW Radars with Low-Cost Backscatter Tags," *Sensors*, vol. 22, p. 2145, 03 2022.
- [17] X. Chen, Z. Li, B. Chen, Y. Zhu, C. X. Lu, Z. Peng, F. Lin, W. Xu, K. Ren, and C. Qiao, "Metawave: Attacking mmwave sensing with meta-material-enhanced tags," in *The 30th Network and Distributed System Security (NDSS) Symposium*. The Internet Society, 2023, pp. 1–17.
- [18] Y. Cao and L. Duan, "Sensing for Jamming in ISAC: Beam Scanning and Beamforming Optimization," *IEEE Transactions on Information Forensics and Security*, vol. 20, pp. 6502–6514, 2025.
- [19] T. Shui, W. Saad, and M. Chen, "Sensing Safety Analysis for Vehicular Networks with Integrated Sensing and Communication (ISAC)," *arXiv preprint arXiv:2505.01688*, 2025.
- [20] D. Li, M. Cai, C.-I. Vasile, and R. Tron, "TLINet: Differentiable Neural Network Temporal Logic Inference," *arXiv preprint arXiv:2405.06670*, 2024.
- [21] Y. Guo, W. Qin, Y. Xu, Y. Gu, C. Yin, and B. Xia, "Predictive Beam Tracking and Power Allocation With Cooperative Sensing for V2I Communication," *IEEE Open Journal of the Communications Society*, vol. 5, pp. 6048–6063, 2024.
- [22] Z. Du, F. Liu, W. Yuan, C. Masouros, Z. Zhang, S. Xia, and G. Caire, "Integrated Sensing and Communications for V2I Networks: Dynamic Predictive Beamforming for Extended Vehicle Targets," *IEEE Transactions on Wireless Communications*, vol. 22, no. 6, pp. 3612–3627, 2023.
- [23] X. Shao, C. You, W. Ma, X. Chen, and R. Zhang, "Target Sensing With Intelligent Reflecting Surface: Architecture and Performance," *IEEE Journal on Selected Areas in Communications*, vol. 40, no. 7, pp. 2070–2084, 2022.
- [24] J. An, C. Xu, D. W. K. Ng, C. Yuen, and L. Hanzo, "Adjustable-Delay RIS Is Capable of Improving OFDM Systems," *IEEE Transactions on Vehicular Technology*, vol. 73, no. 7, pp. 9927–9942, 2024.
- [25] W. Yuan, L. Zhou, S. K. Dehkordi, S. Li, P. Fan, G. Caire, and H. V. Poor, "From OTFS to DD-ISAC: Integrating sensing and communications in the delay doppler domain," *IEEE Wireless Communications*, 2024.
- [26] R. Li, X. Shao, S. Sun, M. Tao, and R. Zhang, "IRS Aided Millimeter-Wave Sensing and Communication: Beam Scanning, Beam Splitting, and Performance Analysis," *IEEE Transactions on Wireless Communications*, vol. 23, no. 12, pp. 19 713–19 727, 2024.
- [27] S. Huang and S. Ontañón, "A Closer Look at Invalid Action Masking in Policy Gradient Algorithms," in *Proceedings of the Thirty-Fifth International Florida Artificial Intelligence Research Society Conference, 2022, Hutchinson Island, Jensen Beach, Florida, USA, May 15-18, 2022*, R. Barták, F. Keshitkar, and M. Franklin, Eds., 2022.
- [28] J. Schulman, F. Wolski, P. Dhariwal, A. Radford, and O. Klimov, "Proximal Policy Optimization Algorithms," *CoRR*, vol. abs/1707.06347, 2017.
- [29] L. Ruff, R. Vandermeulen, N. Goernitz, L. Deecke, S. A. Siddiqui, A. Binder, E. Müller, and M. Kloft, "Deep one-class classification," in *International conference on machine learning*. PMLR, 2018, pp. 4393–4402.
- [30] O. Maler and D. Nickovic, "Monitoring temporal properties of continuous signals," in *Formal Techniques, Modelling and Analysis of Timed and Fault-Tolerant Systems*, Y. Lakhnech and S. Yovine, Eds. Berlin, Heidelberg: Springer Berlin Heidelberg, 2004, pp. 152–166.
- [31] D. Li, M. Cai, C.-I. Vasile, and R. Tron, "Learning Signal Temporal Logic through Neural Network for Interpretable Classification," in *2023 American Control Conference (ACC)*, 2023, pp. 1907–1914.
- [32] D.-H. Lee et al., "Pseudo-label: The simple and efficient semi-supervised learning method for deep neural networks," in *Workshop on challenges in representation learning, ICML*, vol. 3, no. 2. Atlanta, 2013, p. 896.
- [33] Q. Ma, J. Zheng, S. Li, and G. W. Cottrell, "Learning representations for time series clustering," *Advances in neural information processing systems*, vol. 32, 2019.
- [34] H. Zha, X. He, C. Ding, M. Gu, and H. Simon, "Spectral relaxation for k-means clustering," *Advances in neural information processing systems*, vol. 14, 2001.